2009

Patterned Well-Ordered Mesoporous Silica Films for Device Fabrication

Todd A. Crosby
University of Massachusetts - Amherst, tcrosby@engin.umass.edu

PATTERNED WELL-ORDERED MESOPOROUS SILICA FILMS FOR DEVICE FABRICATION

A Thesis Presented
by

TODD ANTHONY CROSBY

Submitted to the Graduate School of the
University of Massachusetts Amherst in partial fulfillment
of the requirements for the degree of

MASTER OF SCIENCE IN CHEMICAL ENGINEERING

September 2009

CHEMICAL ENGINEERING

PATTERNED WELL-ORDERED MESOPOROUS SILICA FILMS FOR DEVICE FABRICATION

A Thesis Presented

By

TODD ANTHONY CROSBY

Approved as to style and content by:

_____
James J. Watkins, Chair

_____
Jeffrey M. Davis, Member

_____
Todd Emrick, Member

_____
Triantafillos J. Mountziaris, Member

_____
Triantafillos J. Mountziaris, Department Head
Chemical Engineering

DEDICATION

To Yuri.

ACKNOWLEDGMENTS

I would like to thank Professor James J. Watkins for his efforts in aiding my professional and personal growth. I am especially thankful for his advice and patience during the tenure of my stay. I would also like to thank my committee members, Professor Jeffrey Davis, Professor Todd Emrick, and Professor Triantafillos J. Mountziaris for their suggestions, advice and time.

I am also grateful for all of my lab members that offered research suggestions, help with various aspects of my project and most importantly friendship. I would also like to mention Dr. Hung-Ting (Tommy) Chen and thank him along with Professor Vince Rotello. Their aid allowed me to finalize the project. I am also thankful for having the chance to work with Dr. John Ell which allowed my project to move in a different direction to produce some exciting new results.

I wish to thank the staff in both the Chemical Engineering and Polymer Science Departments at the University of Massachusetts, namely Bobbi Bassett and Barbara Bou, for their efforts that range from making the process smoother to handling my daily questions. I would also like to thank Lou, Sekar and Jack for being there to answer question after question about TEM, X-ray, SAXS, AFM and XPS.

I am extremely grateful for my parents, Bob and Cindy, who gave me the start I needed to find my way through life and were always there to offer support and understanding in whatever path I chose. Finally, I wish to thank my girlfriend Yuri for giving me the motivation to finish as well offering limitless support and kindness.

ABSTRACT

PATTERNED WELL-ORDERED MESOPOROUS SILICA FILMS FOR DEVICE FABRICATION

September 2009

TODD ANTHONY CROSBY, B.S., UNIVERSITY OF PITTSBURGH

M.S.Ch.E., UNIVERSITY OF MASSACHUSETTS AMHERST

Directed by: Professor James J. Watkins

Developing effective methods of generating thin metal oxide films are important for sensing and separations applications. An obstacle to device fabrication is controlling the size and spatial orientation of domain level pores while retaining the ability to generate arbitrary device level patterns. Well-ordered hexagonally packed cylindrical pores were created by taking advantage of block copolymer self-assembly followed by selective condensation of silica precursors using supercritical carbon dioxide as the solvent. It was possible to control the pore size by choosing PEO-PPO-PEO (Pluronic® series) triblock copolymers of differing molecular weights.

These processes were then incorporated with conventional lithographic techniques to generate patterns on the device scale. The first route involves replacement of the organic acid catalyst with a photoacid generator that restricts acid formation by masking pre-determined regions then exposing to UV light. The second route is similar except that addition of a cross-linking agent limits acid diffusion while reversing the tone of the

final pattern. The third route avoids acid diffusion altogether and generates the pattern through reactive ion etching through a sacrificial photoresist. A completely different fourth route was taken and nanoimprint lithography was used to generate sub-micron patterns with alternate block copolymers.

The feasibility of the preliminary devices generated in this thesis has been examined through particle diffusion experiments. Samples were soaked in a fluorescent dye then exposed to multiple sizes of gold nanoparticles. Fluorescence quenching was then monitored to determine pore accessibility.

TABLE OF CONTENTS

Page

LIST OF TABLES

Table Page

LIST OF FIGURES

Figure Page

CHAPTER 1

INTRODUCTION

1.1 Overview

The long-term goal of this project was to develop methodologies using supercritical carbon dioxide mediated silica block copolymer infusion paired with current device scale patterning technologies for fabrication of multi-scale devices. Stemming from this objective are three shorter term goals – the first of which includes expanding previous work on supercritical fluid mediated infusion to other block copolymer templates. Following this, a variety of patterning techniques were examined and tested for viability and compatibility with this infusion process. These processes include conventional lithography/reaction ion etching, direct patterning via optical lithography and nanoimprint lithography. Finally, the feasibility of these devices as separations media was examined using a particle diffusion separation experiment. The research in this dissertation is the basis for developing a structure that can further be modified for sensing and microfluidic applications.

The motivation and science behind the project along with current research in the sensing and microfluidic areas are outlined in Chapter 1. The polymer physics behind ordering the block copolymer templates and the thermodynamics involved with the supercritical fluid infusion are described. The characterization tools utilized in this study are also detailed in this chapter.

Chapter 2 describes procedures to develop smooth mesoporous silica thin films using a variety of poly(ethylene oxide)-b-poly(propylene oxide)-b-poly(ethylene oxide) (PEO-b-PPO-b-PEO, Pluronic®) block copolymers that yield morphologies of hexagonally packed cylinders aligned parallel to the substrate. Template order is induced through the addition of homopolymers that can hydrogen bond to the PEO domains. The polymer templates were then replicated by acid catalyzed selective metal oxide infusion into the hydrophilic domains using supercritical carbon dioxide as the solvent. Two separate techniques for this infusion process are also described.

Methods of patterning the materials *via* optical lithography are described in Chapter 3. The samples are directly patterned using a photo acid generator that generates acid upon UV exposure. The acid then catalyzes the silica condensation in those specific regions Conventional photoresist lithography followed by reactive ion etching is also utilized to generate ordered mesoporous silica patterns. The limitations and utility of each method are described.

Chapter 4 focuses on nanoimprint lithography into PHEMA homopolymer and PMMA-PHEMA diblock copolymer. This patterning technique enables smaller feature sizes and bypasses some disadvantages associated with the optical lithographic methods at the cost of some template limitations. The current work and future potential for this process are detailed within the chapter.

The fabricated devices are examined in Chapter 5. Nanoparticle segregation is tracked by quenching fluorescent dye with different sized gold nanoparticles. A fluorescent dye is impregnated into well-ordered patterned mesoporous silica films then

the film is placed in nanoparticles solutions of known concentrations and sizes while examined via optical microscopy. This chapter examines the feasibility and utility of the devices developed within this dissertation.

Chapter 6 summarizes the conclusions and discusses future work.

1.2 Motivation

Mesoporous metal oxide films have been utilized for microelectronics, sensors, separations, and catalysis.[1-5] Controlled cost-efficient patterning of metal oxide films, that will generate device level structures while maintaining inherent porosity, increases the utility of these systems. There is a great amount of interest in chemically modified porous metal oxide films, especially SiO_2.[6-9] Humidity sensors have been developed based on thin films of silica nanoparticle aerogels[10] and lithium doped mesoporous silica MCM-41.[11] The application of gas sensors changes with the metal oxide – SnO_2 has been used as an NO_2 sensor,[12] ZnO is used as a sensor for CO,[13] while In_2O_3 is used for methane.[14]

Mesoporous silica structures are also being examined for their utility in microfluidics and separations.[15-17] It is important to note that an important application of nanofluidic devices is in the area of separation science. For example, arrays of regularly-spaced micrometer scale pillars have been used to separate long DNA molecules with some success but have not reached the efficiency of pulsed field gel electrophoresis. It is predicted that nanometer scaled devices will aid in this endeavor.[18] Furthermore, mesoporous silica membranes have been examined as separation membranes.

Mesoporous silica was templated using surfactants within an anodic alumina membrane using evaporation induced self-assembly (EISA). It was shown the device with 3.4 nm channel diameter successfully excluded myoglobin (~4.0 nm) and bovine serum albumin (BSA, ~7.2 nm) but allowed rhodamine B (~1 nm) and vitamin B12 (~2.4 nm) to pass through.[19] More recently, our work demonstrated size exclusion within mesoporous silica that was templated from Pluronic F127/PAA mixtures and formed by selective $scCO_2$ mediated TEOS infusion. Cylindrical pores of approximately 7 nm in diameter excluded 14 nm core GNPs but allowed 2 nm core GNPs inside of the pore to quench a fluorescent dye. [20]

Sensing and micro-/nanofluidic applications require domain level orientation as well as device level patterning. One motivation behind this dissertation lies in further developing new devices by controlling spatial orientation of silicon dioxide mesopores while retaining the ability to generate device level patterns. Another focus is demonstrating accessibility of the nanochannels that lie parallel to the substrate while utilizing methods that will comparatively reduce process times and employ inexpensive, easily accessible materials.

1.3 Typical Device Fabrication Techniques

There are numerous methods to form patterned structures in the nanometer range including micromolding in capillaries (MIMIC),[21-25] electron-beam (e-beam) lithography,[26] direct UV or X-ray lithography[27-31], dip-pen nanolithography (DPN),[32-34] and conventional lithography.[35, 36] Direct-write methods such as e-beam lithography and

DPN while accurate and useful for any type of geometry are time consuming when generating patterns in large areas. However, contact molding such as nanoimprint lithography (NIL) can pattern arbitrary submicron features on a relatively large scale at reduced costs and expediated processing times.[37] The formation of mesoporous structures in many of these technologies is driven by the principle of evaporation-induced self-assembly (EISA), which is an equilibrium result from interfacial interaction and silica condensation.[38] EISA complicates formation of patterns with desired mesoporous morphology in certain applications. It would be advantageous if template assembly was separate from that of patterning and replication. This would enable the use of a wider variety of polymer templates. Patterning an amphiphilic diblock copolymer and pairing this with supercritical carbon dioxide ($scCO_2$) mediated metal oxide infusion allows for mechanically stable patterned porous metal oxide films of arbitrary device scale geometry. Furthermore, formation of the polymer template is separate from that of the metal oxide deposition enabling a wide array of mesoporous structures.[39-41] An efficient method of pattering mesoporous silica films with controllable pore orientation is in demand for the applications that involves utilization of confined nanospace.

1.4 Ordering Block Copolymer Templates

Synthesizing well-defined nanoporous metal oxide films is not a trivial task and is one of the early hurdles that must be overcome on the path to developing a functional device. Nevertheless, films of mesoporous silicates have been developed using diblock copolymers as templates in supercritical carbon dioxide ($scCO_2$) thus validating the

concept.[39, 40] Pai *et al.*[40] developed a procedure for depositing metal oxide films via condensation within a self-assembling block copolymer with hydrophobic and hydrophilic domains.[39, 40] The initial step is to spin-coat a block copolymer solution that will result in a specified structure.[42] Figure 1 shows a calculated phase diagram for an AB linear block copolymer. The morphology is tunable through the Flory-Huggins interaction parameter (χ), degree of polymerization (N), and the volume fraction (f). Once annealed, the block copolymer self assembles into the appropriate morphology.

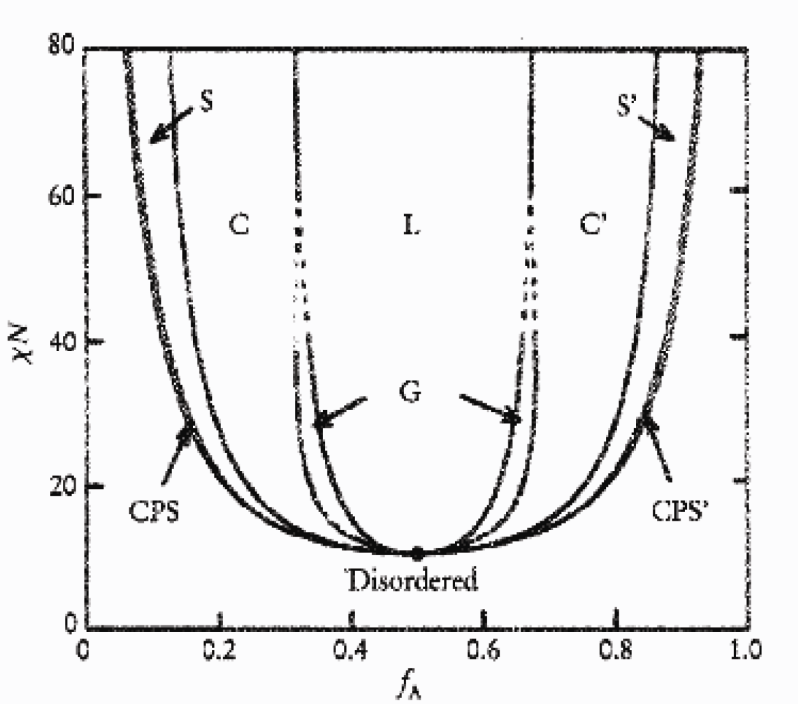

Figure 1.1: Theoretical phase diagram for linear copolymers. Mean-field theory predicts Cylindrical (C), Spherical (S), Lamellar (L), and Gyroid (G) morphologies. The morphology of the block copolymer template is tunable given the interaction parameter, degree of polymerization and composition.[42]

1.5 Supercritical Carbon Dioxide Mediated Metal-oxide Infusion

Carbon dioxide has a relatively easily accessible critical point of about 74 bar (1075 psi) and 31.1 °C and is inexpensive and relatively benign when compared to organic solvents. Supercritical fluids have significant advantages over solution based methods. CO_2 will solvate small molecules (such as alkoxides and metal oxides) at increased pressures while it is a poor solvent for the polymer templates. The density is tunable and can approach that of liquid solvents. At higher pressures the supercritical CO_2 slightly swells or dilates the polymer increasing diffusivity and allowing the metal oxide to penetrate the polymer.

Figure 2 shows accessible densities and compares the surface tension of CO_2 to water and a common organic solvent (hexane). This process combines the advantages of a gas with the advantages of a liquid. Again, reacting under zero surface tension and slight swelling implies that the mesostructure will not be disturbed during this process. Furthermore, the ability to deliver large amounts of precursor stems from reaching liquid-like densities.

In order to replicate the polymer with a metal oxide the reaction should only occur within a single domain of the block copolymer. The chemistry is controlled by utilizing a block copolymer that has both hydrophobic and hydrophilic domains. A catalytic amount of hydrophilic organic acid is introduced into the amphiphilic copolymer/solvent mixture. Introduction of supercritical carbon dioxide then slightly dilates the polymer and allows a metal oxide to gently infiltrate both domains but

selectively react in the region that is doped with an acid catalyst. In short, the reaction is limited to a single domain and mimics the block copolymer morphology.

After infusion of the metal oxide, the polymer template can then be removed and the silica is further condensed through calcination, leaving only the 3D replicate. Depending on the degree of condensation some shrinkage of the template will occur but the structure does not collapse at 400 °C.[39, 40] Techniques such as lithography can be implemented into this procedure to control the structure on a variety of length scales. Patterning of the substrate is possible while simultaneously controlling the nanoscale morphology through self assembly. [39] This technique offers a rapid method of designing a variety of morphologies without a significant increase in cost.

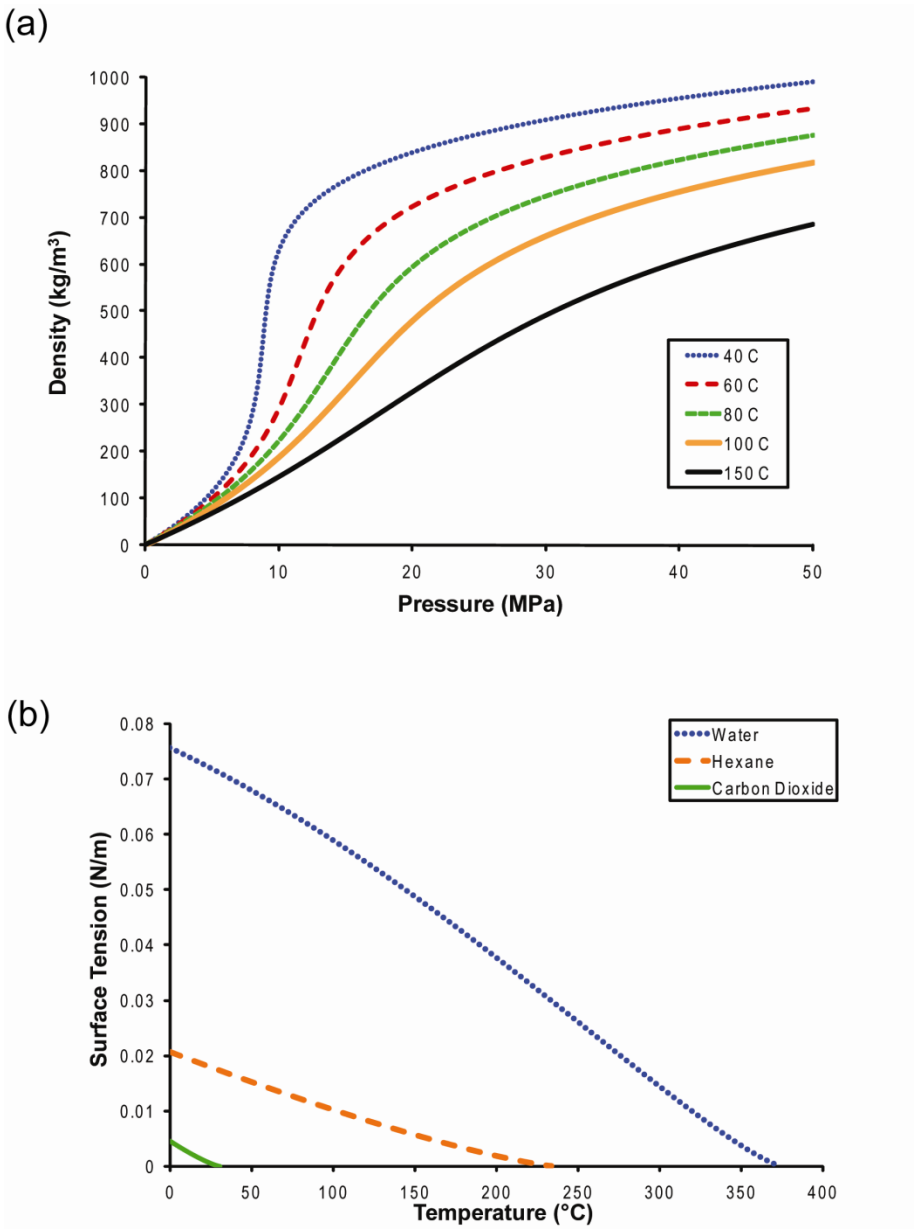

Figure 1.2: (a) The density of carbon dioxide as a function of pressure and temperature. (b) Comparison between water, hexane and CO_2. It is possible to obtain liquid-like densities while retaining gas-like properties. Adapted from NIST webbook.

1.6 Characterization Tools

A variety of characterization tools will be utilized in this project. A working knowledge of the fundamentals and understanding the purpose and limits of each instrument are required to analyze the devices developed within this project

1.6.1 X-ray Diffraction

The basis of forming the mesoporous channels lies in phase-segregation of block copolymers. X-ray Diffraction at small angles (XRD) requires a difference in electron densities for an appropriate signal. Condensing silica in one block then thermally degrading the other block to form voids drastically increases the contrast (voids have essentially zero electron density) and enables smooth thin films to be analyzed. XRD spectra was collected using a PANalytical X'Celerator using Cu Kα-radiation (λ=0.154 nm) with a 1/16 divergence slit and copper filter to protect the detector at low angles. The center to center distance or d-spacing is determined using the position of the strong (100) peak and Bragg's Law ($d=n\lambda(2\sin\theta)$).[43]

1.6.2 Transmission Electron Microscopy

In order for transmission electron microscopy (TEM) to be effective, the sample thickness must be at least less than 0.5 μm but optimally less than 100 nm. The difficulty of gathering an image scales with the thickness. Thick sections will scatter electrons reducing the amount that transmits through the sample causing the image to be dark. A

hole is the most efficient transmitter of electrons meaning voids are the brightest.[43] TEM specimens of mesoporous silica patterns were prepared by scraping material from the substrate. The scraped material is ground, suspended in ethanol, and then transferred on a carbon-coated copper grid to be examined using a JEM-2000FX II.

1.6.3 Scanning Electron Microscopy

A scanning electron microscope (SEM) functions around the interaction of a beam of electrons with a solid surface. Silica samples are only semi-conductive and collect charge that will interfere with the incoming electron beam. To avoid sample charging a thin layer of gold or platinum is deposited.[43] The silica samples were prepared by splitting the wafer and mounting the sample perpendicularly in a trench using a silver paste. The mounts were then platinum coated for 4 minutes and images were collected using a JSM-6320 FXV.

1.6.4 Profilometry

Film thickness was measured via profilometry. The profilometer simply traces (at a known force) the surface with a 12.5 µm tip in measuring differences in height. Height differences were generated in the film by either scoring sections of the silica post calcination or by wiping sections of the substrate coated with the block copolymer template with a solvent before infusion to prevent deposition.

1.6.5 Atomic Force Microscopy

A Digital Instruments Nanoscope III Atomic Force Microscope (AFM) in tapping mode was also utilized to measure height differences. The samples were analyzed under ambient conditions using silicon cantilevers with a spring constant of 0.58 N/m. In tapping mode the AFM cantilever oscillates and the resulting tip-sample forces generate the image. This tool has the advantage of generating three dimensional images compared to the 2D images from profilometry along with being able to probe smaller feature sizes and modulus variations.

1.6.6 Attenuated Total Reflection Fourier Transform Infrared Spectroscopy

Attenuated Total Reflection Fourier Transform Infrared Spectroscopy (ATR-FTIR) spectra were collected using a Nicolet 6700 FT-IR spectrometer equipped with a Harrick grazing angle ATR accessory (GATR) and a liquid nitrogen cooled photovoltaic detector (LN-MCT). Spectra were recorded under a steady nitrogen (N2) flow to limit absorbance peaks due to residual water and CO_2 at 128 scans with a 4 cm^{-1} resolution. The penetration distance is approximately one micrometer and all samples were less than 400 nm film thickness.

1.6.7 X-ray Photoelectron Spectroscopy

X-ray photoelectron spectroscopy wa s performed using a Quantum 2000 ESCA Microprobe. The source is monochromatic Al Kα X-rays (1486.6 KeV) and the device is equipped with an Ar+ ion-sputtering gun. In each case a spectral analysis is followed by

a sputtering analysis. XPS is destructive and sputters into a sample using an ion beam. Typical spectral settings include a survey with X-rays at 200u50W15kV and a time of 4 minutes and 185 eV. The sputtering settings are 70 cycles with 0.5 minute intervals with a setting of 500V1x1 and 46 eV for a 100 nm film. The detector is set for a take-off angle of 45°.

1.6.8 Optical Microscopy (Fluorescence) and Confocal Microscopy

An optical microscope was also used to characterize samples. Reflection mode was used given that the substrate was a silicon wafer. Indicating dyes were viewed via fluorescence. Confocal Laser Scanning Microscopy (CLSM) has the advantage of probing fluorescent materials by combining thin slices of a sample to form a 3D image.

1.7 References

(1) A. Corma, *Chemical Reviews (Washington, D. C.)* **1997**, 97, 2373-2419.

(2) M. E. Davis, *Nature* **2002**, 417, 813-821.

(3) F. Schuth, W. Schmidt, *Advanced Materials* **2002**, 14, 629-638.

(4) A. Stein, *Advanced Materials* **2003**, 15, 763-775.

(5) G. Wirnsberger, P. D. Yang, B. J. Scott, B. F. Chmelka, G. D. Stucky, *Spectrochimica Acta, Part A: Molecular Spectroscopy* **2001**, 57, 2049-2060.

(6) B. J. Melde, B. J. Johnson, P. T. Charles, *Sensors* **2008**, 8, 5202-5228.

(7) F. Wang, J. Yang, K. Wu, *Analytica Chimica Acta* **2009**, 638, 23-28.

(8) S. D. Alvarez, A. M. Derfus, M. P. Schwartz, S. N. Bhatia, M. J. Sailor, *Biomaterials* **2009**, 30, 26-34.

(9) B. Yuliarto, Y. Kumai, S. Inagaki, H. Zhou, *Sensors and Actuators B* **2009**, 138, 417-421.

(10) W. C. Wang CT, Chen IC, Huang YH`, *SENSORS AND ACTUATORS B-CHEMICAL* **2005**, 107, 402-410.

(11) L. Wang, D. Li, R. Wang, Y. He, Q. Qi, Y. Wang, T. Zhang, *Sensors and Actuators B* **2008**, 133, 622-627.

(12) J. Zhang, S. Wang, Y. Wang, Y. Wang, B. Zhu, H. Xia, X. Guo, S. Zhang, W. Huang, S. Wu, *Sensors and Actuators B* **2009**, 135, 610-617.

(13) C.-Y. Liu, C.-F. Chen, J.-P. Leu, *Journal of The Electrochemical Society* **2009**, 156, J16-J19.

(14) T. Waitz, T. Wagner, T. Sauerwald, C.-D. Kohl, M. Tiemann, *Advanced Functional Materials* **2009**, 19, 653-661.

(15) A. Paul, M. Sarkar, D. C. Khara, T. Kamijo, A. Yamaguchi, N. Teramae, A. Samanta, *Chemical Physics Letters* **2009**, 469, 71-75.

(16) C. C. Striemer, T. R. Gaborski, J. L. McGrath, P. M. Fauchet, *Nature* **2007**, 445, 749-753.

(17) M. M. Kulkarni, R. Bandyopadhyaya, A. Sharma, *Journal of Chemical Sciences* **2008**, 120, 637-643.

(18) J. C. T. Eijkel, A. v. d. Berg, *Microfluid Nanofluid* **2005**, 1, 249-267.

(19) A. Yamaguchi, N. Teramae, *Analytical Sciences* **2008**, 24, 25-30.

(20) H.-T. Chen, T. A. Crosby, M.-H. Park, S. Nagarajan, V. M. Rotello, J. J. Watkins, *Journal of Materials Chemistry* **2009**, 19, 70-74.

(21) P. Innocenzi, T. Kidchob, P. Falcaro, M. Takahashi, *Chemistry of Materials* **2008**, 20, 607-614.

(22) M. Trau, N. Yao, E. Kim, Y. Xia, G. M. Whitesides, I. A. Aksay, *Nature* **1997**, 390, 674-676.

(23) P. D. Yang, T. Deng, D. Y. Zhao, P. Y. Feng, D. Pine, B. F. Chmelka, G. M. Whitesides, G. D. Stucky, *Science* **1998**, 282, 2244-2246.

(24) P. D. Yang, A. H. Rizvi, B. Messer, B. F. Chmelka, G. M. Whitesides, G. D. Stucky, *Advanced Materials* **2001**, 13, 427-431.

(25) P. D. Yang, G. Wirnsberger, H. C. Huang, S. R. Cordero, M. D. McGehee, B. Scott, T. Deng, G. M. Whitesides, B. F. Chmelka, S. K. Buratto, G. D. Stucky, *Science* **2000**, 287, 465-467.

(26) G. G. Della, M. Guglielmi, G. Brusatin, M. Prasciolu, F. Romanato, *Journal of Sol-Gel Science and Technology* **2008**, 48, 212-216.

(27) F. Cagnol, D. Grosso, G. Soler-Illia, E. L. Crepaldi, F. Babonneau, H. Amenitsch, C. Sanchez, *Journal of Materials Chemistry* **2003**, 13, 61-66.

(28) A. M. Dattelbaum, M. L. Amweg, L. E. Ecke, C. K. Yee, A. P. Shreve, A. N. Parikh, *Nano Letters* **2003**, 3, 719-722.

(29) D. A. Doshi, N. K. Huesing, M. C. Lu, H. Y. Fan, Y. F. Lu, K. Simmons-Potter, B. G. Potter, A. J. Hurd, C. J. Brinker, *Science* **2000**, 290, 107-111.

(30) Y. F. Lu, Y. Yang, A. Sellinger, M. C. Lu, J. M. Huang, H. Y. Fan, R. Haddad, G. Lopez, A. R. Burns, D. Y. Sasaki, J. Shelnutt, C. J. Brinker, *Nature* **2001**, 410, 913-917.

(31) L. Malfatti, T. Kidchob, S. Costacurta, P. Falcaro, P. Schiavuta, H. Amenitsch, P. Innocenzi, *Chemistry of Materials* **2006**, 18, 4553-4560.

(32) S. H. Hong, J. Zhu, C. A. Mirkin, *Science (Washington, D. C., 1883-)* **1999**, 286, 523-525.

(33) C. A. Mirkin, *Science (Washington, D. C., 1883-)* **1999**, 286, 2095-2096.

(34) R. D. Piner, J. Zhu, F. Xu, S. H. Hong, C. A. Mirkin, *Science (Washington, D. C., 1883-)* **1999**, 283, 661-663.

(35) F. K. de Theije, A. R. Balkenende, M. A. Verheijen, M. R. Baklanov, K. P. Mogilnikov, Y. Furukawa, *Journal of Physical Chemistry B* **2003**, 107, 4280-4289.

(36) J. A. Paik, S. K. Fan, C. J. Kim, M. C. Wu, B. Dunn, *Journal of Materials Research* **2002**, 17, 2121-2129.

(37) J. Y. Cheng, C. A. Ross, H. I. Smith, E. L. Thomas, *Advanced Materials* **2006**, 18, 2505-2521.

(38) C. J. Brinker, Y. F. Lu, A. Sellinger, H. Y. Fan, *Advanced Materials* **1999**, 11, 579-585.

(39) R. A. Pai, R. Humayun, M. T. Schulberg, A. Sengupta, J.-N. Sun, J. J. Watkins, *Science* **2004**, 303, 507-510.

(40) R. A. Pai, J. J. Watkins, *Advanced Materials* **2006**, 18, 241-245.

(41) V. R. Tirumala, R. A. Pai, S. Agarwal, J. J. Testa, G. Bhatnagar, A. H. Romang, C. Chandler, B. P. Gorman, R. L. Jones, E. K. Lin, J. J. Watkins, *Chemistry of Materials* **2007**, 19, 5868-5874.

(42) F. S. Bates, Fredrickson, G. H., *Physics Today* **1999**, 52, 32-38.

(43) D. Campbell, J. R. White, *Polymer Characterization: Physical Techniques*. 1989, London: Chapman and Hall. 154-189, 191-238, 242-269.

CHAPTER 2

MANIPULATING DOMAIN SIZE OF WELL-ORDERED MESOPOROUS SILICA THIN FILMS

2.1 Introduction

Well-ordered mesoporous silica thin films have numerous applications as sensors[1-5] and separation devices.[6] Previous work within the group has shown that it is possible generate well-ordered mesoporous silica thin films using triblock surfactants of poly(ethylene oxide)-block-poly(propylene oxide)-block-poly(ethylene oxide) (PEO-PPO-PEO) as templates.[7, 8] For device fabrication, it would be advantageous to have cylindrical channels aligned parallel to the substrate over a relatively long range. A mesoporous silica film with channels parallel to the substrate that has increased long range order has been fabricated through use of a homopolymer that will strongly bond to one block of the polymer. In this case, poly(acrylic acid) (PAA) or poly(4-hydroxystyrene) (PHOST) will hydrogen bond to the PEO block of Pluronic® F127 (PEO_{106}-PPO_{70}-PEO_{106}). Note that because template formation and silica deposition are decoupled, a range of suitable templates are accessible.[7-10] Furthermore, channel diameters can be tailored over broad ranges by adjusting template molecular weight.[11] This previous work will act as the starting point for this project.

2.2 Experimental

2.2.1 Equipment

Mesoporous silica films were generated using the supercritical CO_2 infusion method described above.[7, 8] The hot wall high pressure reactor consists of two stainless steel hubs sealed with a graphite ring (55 ft-lb torque) purchased from Grayloc® Products. Heating bands (Watlow) attached to the reactor walls are used to control the gas temperature. Internal reactor volume is approximately 140 mL. There are 4 ports drilled into the reactor cap, one for measurement of the internal pressure, another for internal temperature, and the carbon dioxide inlet and outlet. There is a safety mechanism installed that will immediately depressurize the system if over-pressurized before vessel failure as well as a thick polycarbonate shield covering the front of the reactor. Figure 2.1 displays a schematic of the reactor. The precursor can be placed inside of the reactor before sealing or injected with CO_2 at any point during the process.

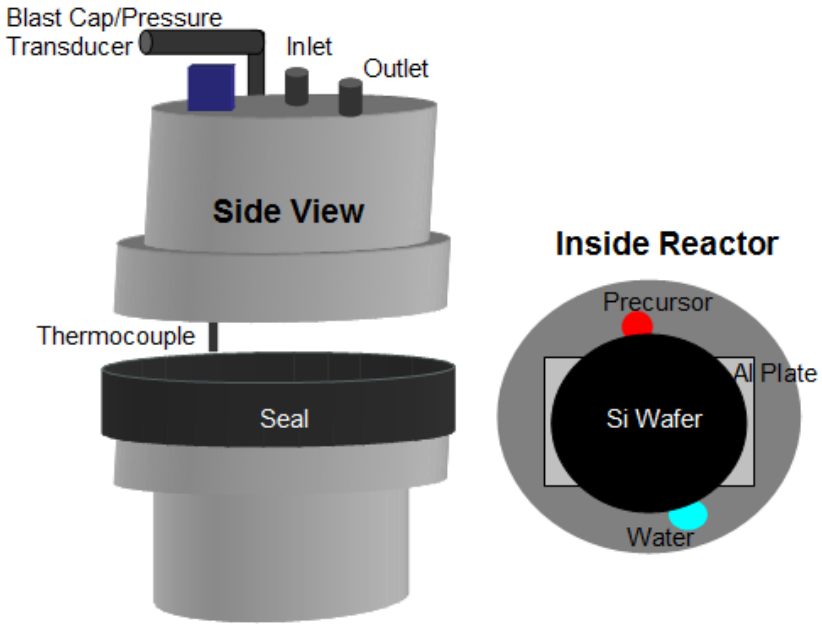

Figure 2.1: Schematic of the high pressure reaction vessel used in the supercritical CO_2 mediated infusion process.

2.2.2 Materials

A polymer blend of inexpensive amphiphilic block copolymers (Pluronic® - BASF) with a hydrogen bonding homopolymer such as PAA (1800 g/mol, Sigma-Aldrich) was used as a template for generating mesoporous silica films with parallel nanochannels. As shown in Figure 2.2, there are a variety of template molecular weights available from BASF that will be utilized to control the resulting pore size. It is important to note that Pluronic F127, F 87, and F 77 all contain 70% (last digit multiplied by 10) of the hydrophilic component (PEO) with decreasing overall molecular weight. The first two digits, when multiplied by 300, correspond to the approximate molecular weight of the hydrophobic component (PPO). The letter designation corresponds to the physical appearance of the material where L stands for liquid, P stands for paste and F for Flakes or solids. Other polymer templates such as polystyrene-block-polyacrylic acid (PS-PAA) and PHEMA-PMMA were synthesized in-house by post-doctoral fellow John

Ell. The catalyst *para*-toluene sulfonic acid (pTSA) was purchased from Sigma-Aldrich and stored in a desiccator. The silica precursor used in all of the experiments is tetraorthoethyl silicate 99% (TEOS) and also purchased from Sigma-Aldrich. Carbon dioxide is bone-dry grade purchased from Air-Gas East. All other solvents were purchased from Sigma-Aldrich and used without further modification.

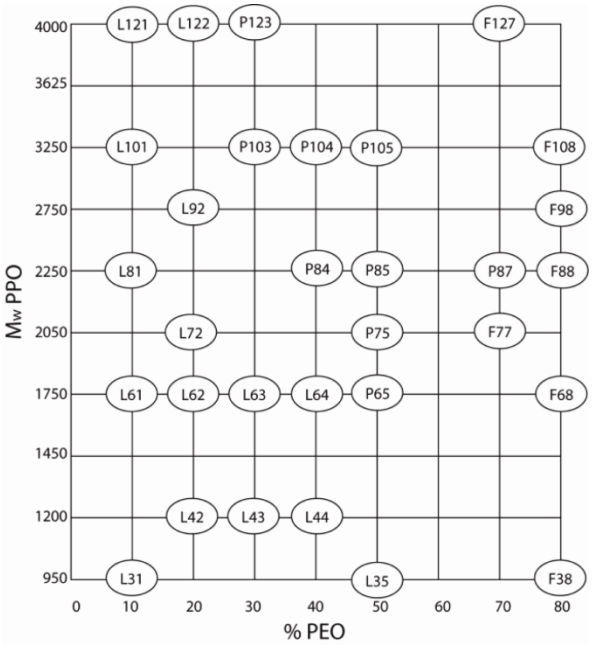

Figure 2.2: The variety of Pluronic® materials available. F127, F87, and F77 will yield cylindrical morphologies while reaching progressively smaller pore sizes. Adapted from BASF. http://www2.basf.us/performancechemical/bcperfpluronic_grid.html

2.2.3 Procedure

2.2.3.1 Sample Preparation

The surfactant solutions (3% mass Pluronic®/mass of solvent) are mixed with 5% pTSA (mass pTSA/mass total solids) and 20% PAA (mass PAA/mass total solids) then

spun-coat (2000 RPM, 60 seconds) onto a silicon substrate from ethanol. Film thickness is a function of solution concentration (which governs viscosity) and spin rate. The film thickness is approximately 300 nm as measured by an interferometer. The sample is then placed onto a 1 cm thick piece of aluminum in the high pressure reactor with 9 μL of TEOS per 50.8 mm diameter wafer on the base of the reactor along with one drop (~25 μm) of distilled water also on the base of the reactor but separated from that of the metal oxide precursor. The reactor and carbon dioxide was either pre-heated before CO_2 injection or heated once a pre-determined amount of CO_2 was in the reactor. Both procedures are described in detail below. Once the reaction is completed the samples were calcined at 400 °C for 6 hours with a heating/cooling ramp rate of 1.67 °C/min.

2.2.3.2 Pre-Heat Method

There are multiple pathways available to reach the reaction conditions – each having different advantages and disadvantages. Pre-heating the reactor and carbon dioxide separately allow time for sample annealing. In the case of PEO based copolymers, this enables any crystallites that have formed at room temperature during the sample preparation to "melt" before the replication process. After spincoating, the sample is placed in the reactor with a drop of water and the reactor is closed but not sealed. The wall heater temperature was set to 78 °C and the system was allowed to equilibrate at a gas temperature of approximately 60 °C. Simultaneously, an ISCO syringe pump filled with CO_2 was pre-heated to 60 °C using a circulating water heater then pressure to 124 bar (~1800 psi). After equilibration the reactor is sealed and the

silica precursor, TEOS, was introduced into the reactor via injection with the $scCO_2$ at the reaction conditions. The reactor was pressurized over 45 min and held at the final conditions for 120 min, then depressurized within 20 min. Figure 2.3 is a schematic of the thermodynamic pathway taken to reach the supercritical reaction conditions.

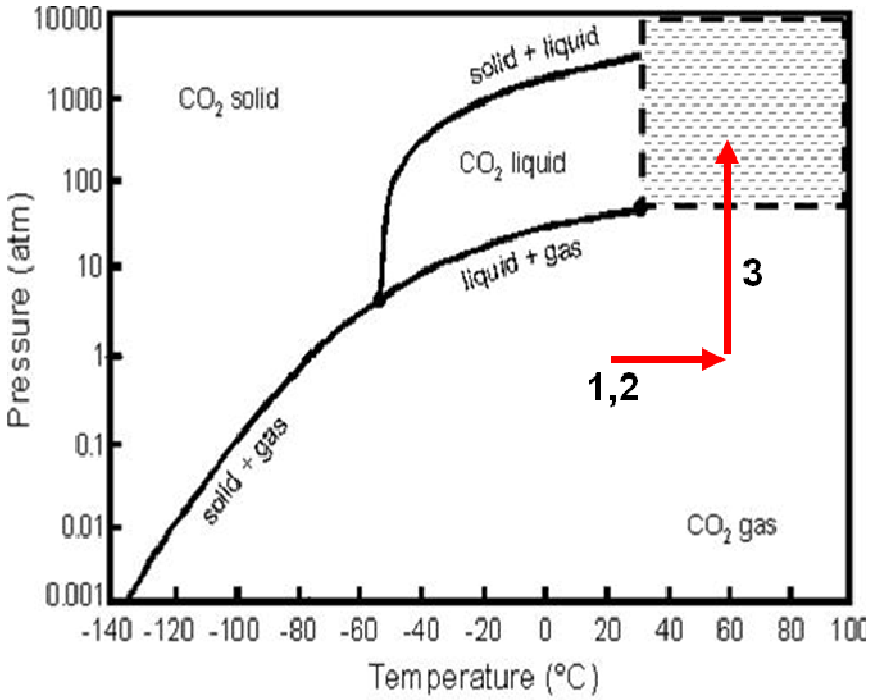

Figure 2.3: Thermodynamic pathway for the pre-heated infusion process. 1.) Sample is placed within the reactor and preheated to 60 °C 2.) CO_2 within the pump is also heated to 60 °C 3.) The pump is set to 124 bar and $scCO_2$ is injected with the precursor.

2.2.3.3 Pre-Injection Method

In cases where annealing is not required or cases where excessive heating is detrimental to the results or stability of the sample it is possible to access supercritical conditions through another path. Instead of pre-heating both the CO_2 and reaction vessel separately, this procedure was adjusted by first injecting CO_2 at room temperature and a

known pressure (above the vapor pressure, typically 70 bar) then heating the reactor to bring the carbon dioxide into the supercritical state. The schematic is shown in Figure 2.4. The precursor is either placed in the reactor before sealing or injected with the room temperature CO_2. It is imperative to calculate the amount of CO_2 required to reach the appropriate pressure at the intended temperature to avoid over-pressurizing the system. This was done using a mass balance where the density of the CO_2 at the final conditions (60 °C, 124 bar) multiplied by the total reactor volume of 140 mL is equivalent to the density of the injected CO2 (Room Temp, 70 bar) multiplied by the volume of CO_2 of interest. Once injected the wall heater is enabled and the system is allowed to react for 2-3 hours. The reactor is then depressurized within 20 minutes and the sample removed for calcination.

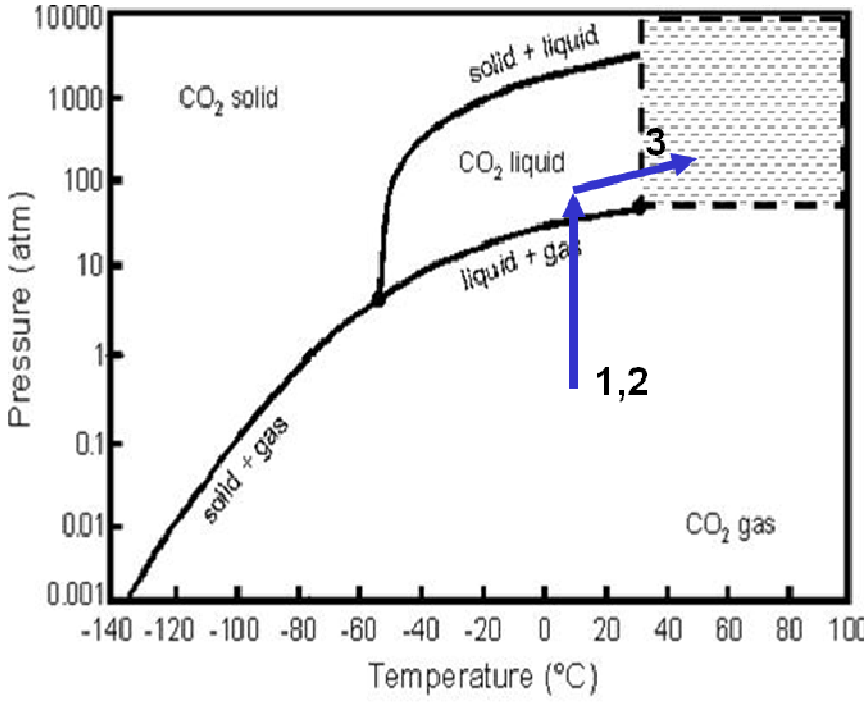

Figure 2.4: Thermodynamic pathway for the Pre-heated Infusion process. 1.) The pump is set to known pressure at a known temperature 2.) The sealed reactor is filled with a predetermined amount of CO_2 3.) The reactor is then heated to the final temperature bring the system to the final pressure.

2.3 Results and Discussion

It is important to note that this method can potentially be used with any amphiphilic copolymer template that microphase segregates. Slight modifications will be necessary depending on the polymer system. It is also possible to thermally or solvent anneal the sample and "freeze" the desired morphology in place before precursor condensation. Furthermore, addition of homopolymer has an influence on the resulting morphology as well as hindering PEO crystallite formation and pore-size effects due to swelling of the PEO block.

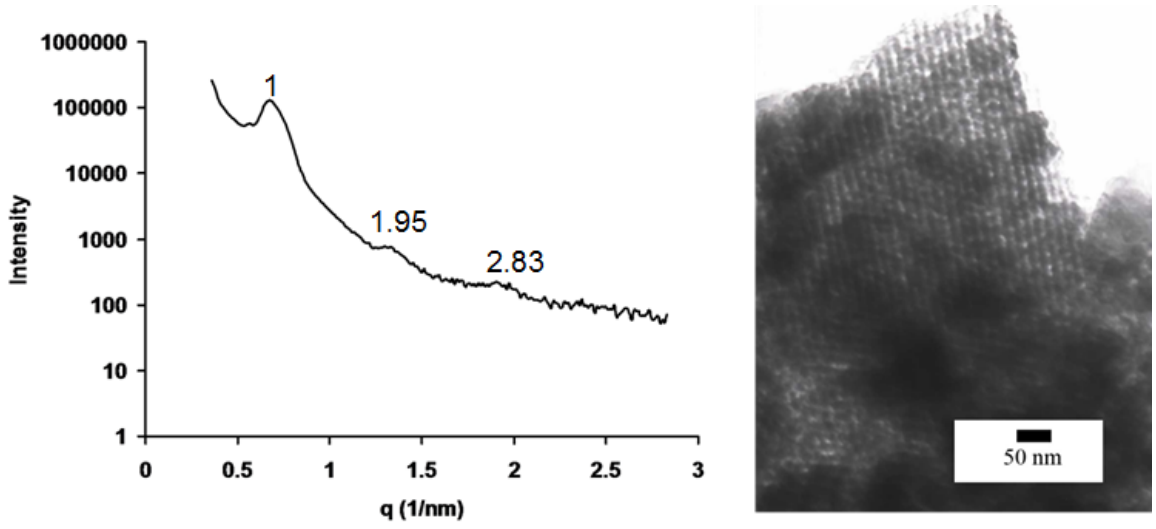

Figure 2.5: Pluronic® F127 templated calcined mesoporous silica. XRD shows peaks at 1, 1.95 and 2.83 which deviate from the ideal of 1, √3, and √7. However, TEM displays that the mesostructure is indeed cylindrical. The d-spacing is 10.4 and the pore domain size is approximated as 7-8 nm.

Three templates are available from BASF that have a molecular weight ratio approaching that required for hexagonally packed cylinders. Pluronic® F127 is the largest of the surfactants containing 70 wt% PEO at an approximate molecular weight of

12,600 g/mol. Following the procedure by Tirumala *et al.*, well-ordered mesoporous silica thin films with cylinders parallel to the surface were generated.[9] X-ray diffraction and transmission electron microscopy were used to characterize the smooth films. Ideal hexagonally packed cylindrical morphology will display normalized XRD peaks at 1, √3, and √7. As shown in Figure 2.5, there are peaks at 1, 1.95, and 2.83 with a Bragg peak yielding a d-spacing of 10.4 nm. This result is similar to that previously discovered within the group.[9] The discrepancy between ideal and actual is attributed to the fact that this is no longer the block polymer but the calcined silica replication. After the swelling induced by the $scCO_2$ mediated infusion process the sample is then calcined and depending on the degree of condensation shrinkage occurs causing the non-ideal behavior. TEM was utilized on numerous samples to confirm that the structures are indeed cylinders parallel to the substrate and are ordered for sections that are at least half a micro in length. The dark sections are SiO_2 that has condensed in the hydrophilic PEO domains whereas the clear areas are pores were PPO has been thermally removed. The pore size as measured using ImageJ from the TEM micrographs is approximately 7-8 nm.

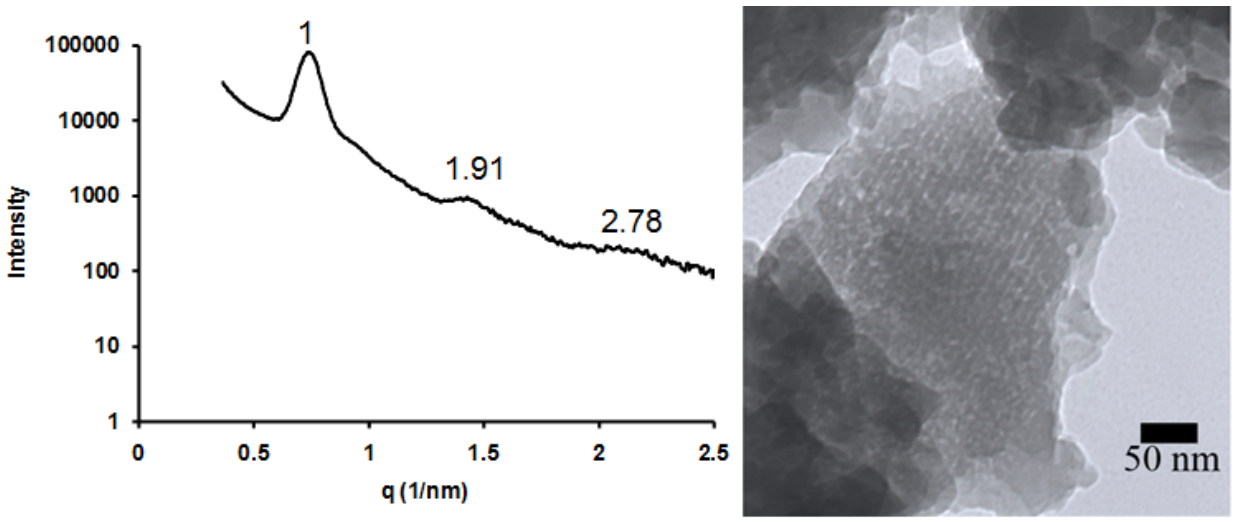

Figure 2.6: Pluronic® F 87 templated calcined mesoporous silica. XRD shows peaks at 1, 1.91 and 2.78 which deviate from the ideal of 1, √3, and √7. Again, TEM displays cylindrical morphology parallel to the substrate The d-spacing is 8.4 and the pore domain size is approximated as 4-5 nm.

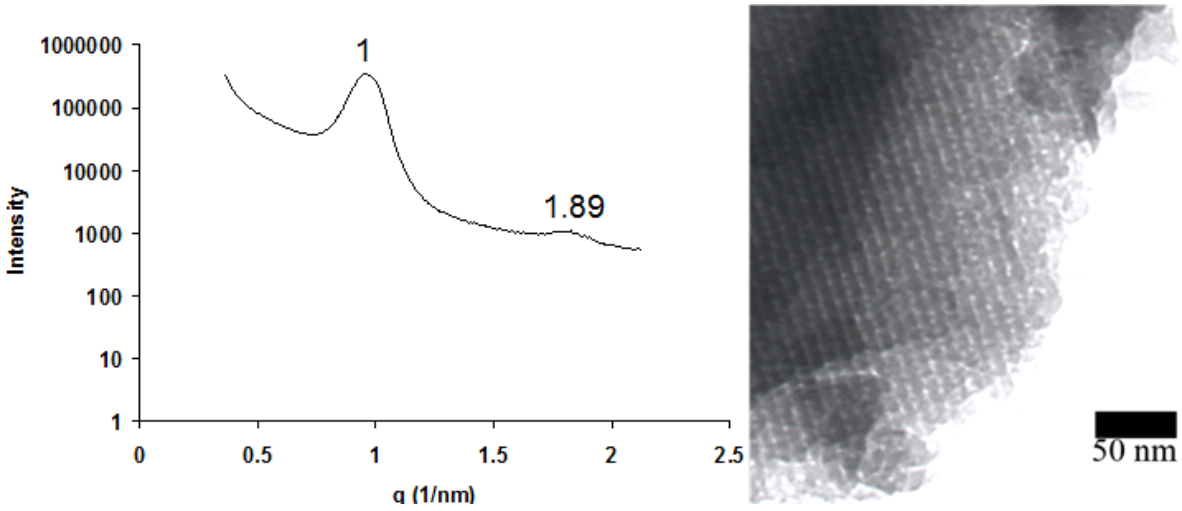

Figure 2.7: Pluronic® F 77 templated calcined mesoporous silica. XRD shows peaks at 1, 1.89. In this case TEM displays well-ordered ocylindrical morphology. The d-spacing is 6.5 and the pore domain size is approximated as 3-4 nm.

The next step was to expand this technique to other PEO-PPO-PEO surfactant copolymers. Pluronic® F 87 has a total molecular weight of approximately 7700 g/mol, about half that as F127. Slightly less TEOS (8 μL) was used during the $scCO_2$ mediated infusion process. The XRD response (Figure 2.6) is extremely similar to that of F127 with peaks of 1, 1.91 and 2.78 but, as expected, the d-spacing is smaller at 8.4 nm. TEM again confirms that the morphology is well-ordered cylinders oriented parallel to the substrate. The channel diameter as measured from the TEM micrograph is 4-5 nm.

The final template available in the desired range is Pluronic® F 77. The total molecular weight of this polymer is approximately 6600 g/mol. Again, as shown in Figure 2.7, XRD displays normalized peaks of 1 and 1.89 but the d-spacing has been reduced to 6.5 nm. TEM also confirms very well-ordered cylindrical morphology with an approximate pore size of 3-4 nm.

2.4 Conclusions

The ability to generate a variety of mesoporous silica channels with $scCO_2$ mediated replication has been demonstrated. The template is ordered prior to the infusion process and induced through addition of homopolymers that can hydrogen bond with the poly(ethylene oxide) block. The pore size is governed by the hydrophobic block and can be controlled by selecting the appropriate molecular weight. The following chapter will describe how to incorporate device fabrication into this process to develop multi-scale structures.

2.5 References

(1) B. J. Melde, B. J. Johnson, P. T. Charles, *Sensors* **2008**, 8, 5202-5228.

(2) J. Tu, R. Wang, W. Geng, X. Lai, T. Zhang, N. Li, N. Yue, X. Li, *Sensors and Actuators B* **2009**, 136, 392-398.

(3) C. T. Wang, C. L. Wu, I. C. Chen, Y. H. Huang, *Sensor and Actuators B - Chemical* **2005**, 107, 402-410.

(4) F. Wang, J. Yang, K. Wu, *Analytica Chimica Acta* **2009**, 638, 23-28.

(5) L. Wang, D. Li, R. Wang, Y. He, Q. Qi, Y. Wang, T. Zhang, *Sensors and Actuators B* **2008**, 133, 622-627.

(6) A. Yamaguchi, N. Teramae, *Analytical Sciences* **2008**, 24, 25-30.

(7) R. A. Pai, R. Humayun, M. T. Schulberg, A. Sengupta, J.-N. Sun, J. J. Watkins, *Science* **2004**, 303, 507-510.

(8) R. A. Pai, J. J. Watkins, *Advanced Materials* **2006**, 18, 241-245.

(9) V. R. Tirumala, R. A. Pai, S. Agarwal, J. J. Testa, G. Bhatnagar, A. H. Romang, C. Chandler, B. P. Gorman, R. L. Jones, E. K. Lin, J. J. Watkins, *Chemistry of Materials* **2007**, 19, 5868-5874.

(10) S. Nagarajan, J. K. Bosworth, C. K. Ober, T. P. Russell, J. J. Watkins, *Chemistry of Materials* **2008**, 20, 604-606.

(11) S. Nagarajan, L. M., R. A. Pai, J. K. Bosworth, P. Busch, D. M. Smilgies, C. K. Ober, T. P. Russell, J. J. Watkins, *Advanced Materials* **2008**, 20, 246-251.

CHAPTER 3

FABRICATING DEVICES FROM PLURONIC TEMPLATED WELL-ORDERED MESOPOROUS SILICA FILMS

3.1 Introduction

There have been previous attempts to directly pattern Pluronic® templates through a modification of conventional optical lithographic techniques. The organic acid was replaced with a photoacid generator (PAG), then the sample was exposed to ultra-violet (UV) light under a photomask which generated a catalytic amount of acid in specific regions. It was found that acid diffusion from exposed PEO to unexposed PEO regions in these surfactant systems was detrimental to pattern retention.[1]

This problem was avoided through use of a specially designed block copolymer, Poly(styrene)-block-poly(*tert*-butyl acrylate) (PS-b-Ptba), that can undergo a chemical transformations when exposed containing PAG. Upon exposure to UV light and generation of acid followed by moderate heating, PtBA is deprotected to form hydrophilic poly(acrylic acid) (PAA). Note that the only the exposed sections are hydrophilic which removes the drive for the acid diffusion into the unexposed regions. The polymer can then be replicated with a metal oxide via the $scCO_2$ mediated process described in Chapter 2. Heating this polymer further generates a cross-linked network of poly(acrylic anhydride) that cannot be infused through $scCO_2$ mediated process. Furthermore, acid can then be generated in the regions that were previously covered by a

mask upon a second mask-less exposure. This reversed system can be infused with silica and generates the opposite tone as described from the previous procedure. Both the negative and positive tones are shown in Figure 3.1.[2]

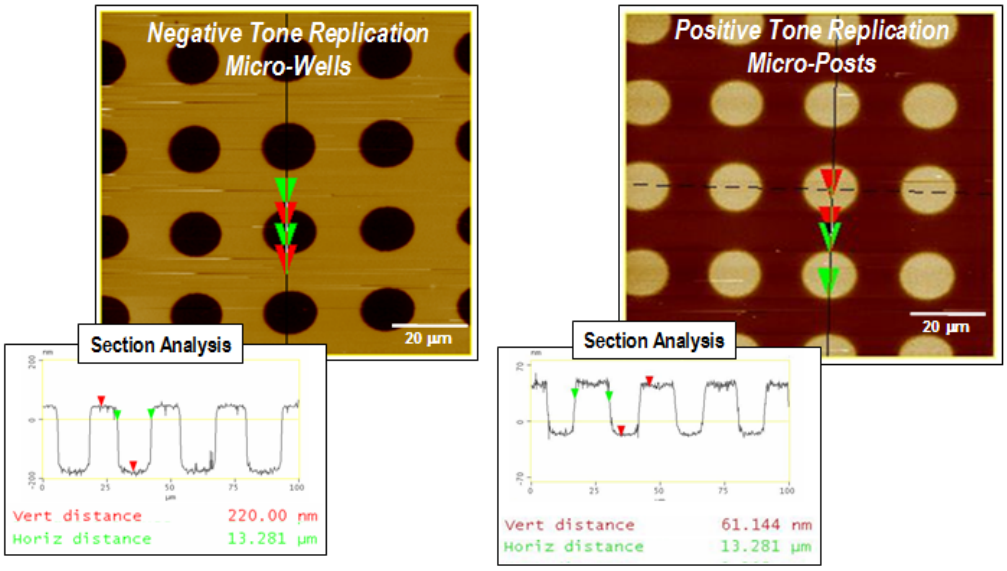

Figure 3.1: Previous work within the group (Nagarajan *et al.*) displaying dual-tone pattered mesoporous silica using a two step chemical amplification process with PS-PtBA block copolymer.

It is important to note that this process is only viable for an amphiphilic block copolymer systems that have the ability to switch from hydrophobic to hydrophilic through chemically amplified mechanisms. In an effort to remove template restrictions but improve pattern retention, an agent was added to induce and mimic the inherent crosslinking action of the PS-PtBA system. The Pluronic® systems were again utilized because they are inexpensive, readily available and have a well-ordered nature. Furthermore, in order to avoid the problem of acid diffusion altogether, a sacrificial photoresist patterned through standard techniques and reactive ion etching were utilized to make patterned samples.

3.2 Experimental

3.2.1 Equipment

A UVP brand shortwave UV bench lamp (15 watt, 0.68 A, 115 V, 60 Hz, 254 nm) was initially used as the UV source to expose the polymer templates. A mask aligner (Microtec SUSS) was then used with an alternate PAG for exposures under vacuum contact.

3.2.2 Materials

All materials were used as received without further modification. Pluronic templates were graciously donated from BASF while all solvents were purchased from Sigma-Aldrich. Two photoacid generators were used in this study: The first being (TPST) which is activated by 254 nm wavelength and second being PAG121 which was donated from CIBA and sensitive over a wide range of UV light. Quartz photomasks were designed in-house and purchased from (name here).

3.2.3 Patterning Procedures

3.2.3.1 Direct Patterning Routes 1 and 2

The initial scheme, that will be the basis of comparison, follows a previously developed method within the group.[1] Solutions of polymer template/homopolymer were used as before, however; a photo-acid generator (such as TPST) replaced the organic acid pTSA. Figure 3.2 displays a schematic of the first route. After the template solution is spun-cast, the resulting film is masked then exposed to UV light. The exposure time, wavelength and intensity will be governed by the PAG requirements. Currently, there are two options available at the university. The first option is a broad mercury lamp centered on 254 nm with only one power setting. The film will be masked by simply placing a quartz photomask on the sample. The second option is a mask aligner (SUSS Microtec) that has the ability for vacuum or proximity mask contact with a narrow source at 365 nm and two power settings. Once acid is generated in the regions that were exposed to UV the sample is reacted with TEOS via the post-injection method. It is important to note that there is nothing to prevent the small molecule acid from diffusing to the unexposed PEO regions. The resulting film is then calcined leaving a mesoporous silica film that has mimicked the mask. Patterned devices will be analyzed using AFM, SEM and optical microscopy.

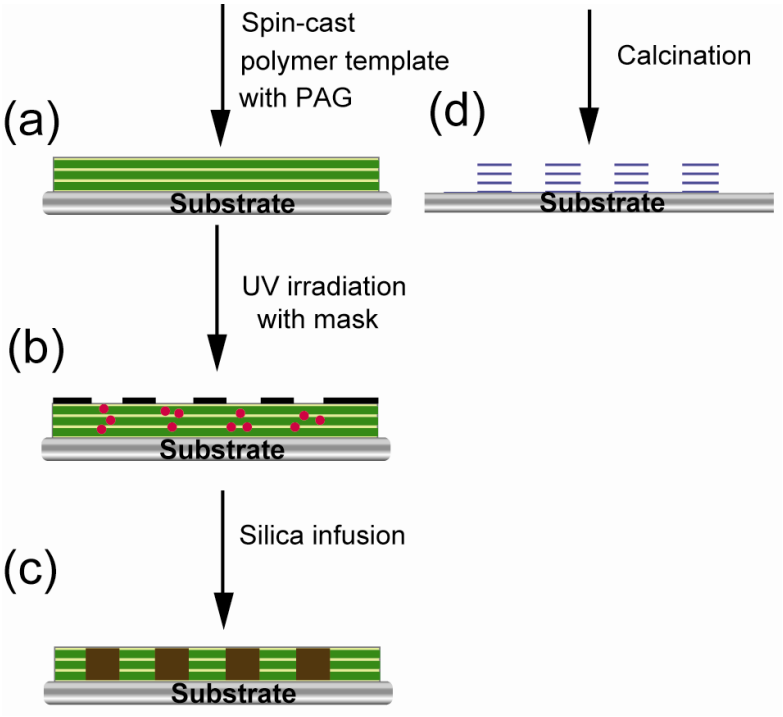

Figure 3.2: Device level patterning – Route 1. (a) A copolymer template is spun-cast with the appropriate homopolymer and PAG. (b) The sample is then masked and irradiated with UV light. (c) The sample is then infused with silica via the cold CO2 method and (d) calcined to remove the polymer template.

The second route (Figure 3.3) is initially the same but is then substantially modified through the addition of a cross linking agent. 1,2,3,6-tetrakis(methoxymethyl) glycouril (TMMGU) is a cross-linking agent that was shown to react with the hydroxyl groups on PAA or PHOST following the addition of acid and moderate heat or at simply very high temperatures.[3] Incorporating this into the solution offers a potential pathway to "shut down" areas of the films to segregate the generated acid. The solution including copolymer template/homopolymer, PAG and cross linking agent is spun onto a silicon substrate per usual. The film is once again UV irradiated under a lithographic mask and acid is generated in the uncovered regions. This film is then immediately heated at 90 °C for 30 seconds to induce crosslinking in acidic regions. Care must be taken when heating

because it is possible to crosslink the unexposed regions with temperatures upwards of 120 °C. Once crosslinked the sample is immediately irradiated without the mask to generate acid in the regions that were previously unexposed. Optimally the crosslinked areas will have completely consumed any acid causing no deposition in those areas while simultaneously acting as a wall that will significantly slow or completely halt any further diffusion. The sample is once again infused with silica via the "cold CO_2" method and calcined at 400 °C. It is important to note that, due to the double exposure, this method results in a pattern that is the inverse of route 1. By utilizing both, it is possible to have both the positive and negative tone regardless of the type of mask used.

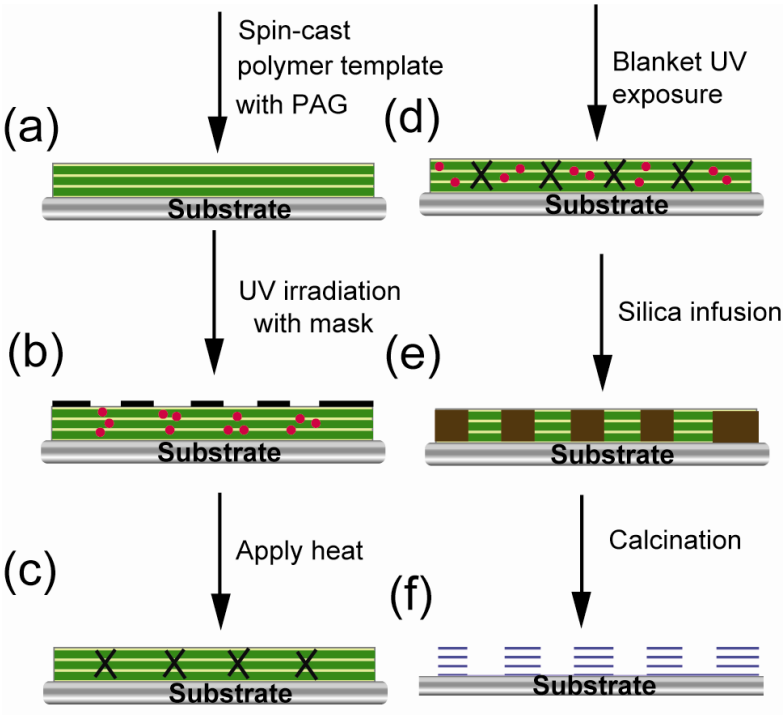

Figure 3.3: Device level patterning – Route 2. (a) A copolymer template is spun-cast with the appropriate homopolymer and PAG. (b) The sample is then masked and irradiated with UV light. (c) The substrate is then annealed for 30 sec at 80 °C to induce crosslinking. (d) Another UV irradiation step is completed without a mask to activate remaining PAG. (e) The sample is then infused with silica via the cold CO2 method and (d) calcined to remove the polymer template.

Two photomasks were used for the patterning. One mask contained 20 um circles and samples using this mask were exposed using a broad UV lamp where the majority of the light is 254 nm. The spuncoat sample contained 3 wt% Pluronic® (mass F127/mass of solvent), 20 wt% PAA (mass of PAA/mass total solids), and 5 wt% TPST (mass of PAG/mass total solids), 1 wt% TMMGU (mass of TMMGU/mass total solids), and was dissolved in ethanol. The substrate was placed approximately 5 cm under the source with the mask placed on top by hand. A 1 cm thick clear quartz plate was placed on top for additional weight. The sample was then exposed for anywhere from 10-30 sec.

The second photomask consisted of lines that range from 8 um to 1 um with a variety of spacing. In order, to successfully pattern smaller feature sizes a cleanroom mask aligner that utilizes vacuum contact was used. Due to the insensitivity of TPST at 365 nm, PAG121 was used. A 3 wt% Pluronic® solution (mass of F127/mass of solvent), with 20 wt% poly(hydroxyl styrene) (mass PHS/mass total solids), 5 wt% PAG121 and 1 wt% TMMGU (mass of TMMGU/ mass total solids) dissolved in 50/50 ethanol/ethyl acetate was used as the template. Under vacuum contact, there was an issue with the substrate adhering to the mask, thus destroying the pattern. Using PHS instead of PAA alleviated this problem due to the more rigid nature (higher glass transition temperature) of PHS. Exposure times ranged from 3 seconds to 3 minutes. Regardless of freezer storage conditions, over an extended time periods PAG121 degrades and requires extremely high exposure energy.

3.2.3.2 Sacrificial Photoresist Route 3

The third route offers a path to avoid the issue of acid diffusion altogether. However, other difficulties arise in trying to obtain extremely sharp features. The first

step, as shown in Figure 3.4, is to generate the mesoporous silica film using the conventional "pre-heated CO_2" method described above. Once the nanochannels are formed photoresist is spun onto the resulting film. The choice of photoresist depends on the mask layout (positive tone or negative tone resist) as well as the target feature size. Both S1813 (Shipley) positive resist and SU8-25 (Microchem) negative resist are readily available. The mesoorous silica film was generated as described above using a system of Pluronic F127/20 wt% PAA/5 wt% pTSA in ethanol. A positive tone photoresist (Shipley S1823) was spun onto the mesoporous silica films at 3000 rpm for 30 sec and baked at 100 °C for 75 sec. Alternatively, a negative tone photoresist could be used to form the inverted structure. The substrate was then exposed with UV light at 365 nm for 4.5 sec using a mask aligner with low vacuum contact. The same quartz mask with 20 µm opaque circles was used for the patterning. After irradiation, the samples were developed using a mixture of water/Developer 351 (v/v = 4:1) yielding an array of pillars with a height of 1.5 µm. The samples were then etched with a Trion Reactive Ion Etcher (RIE) at a pressure of 100 mTorr (13.3 Pa) with an RIE setting of 150 watts. Etching time ranged from 5 to 40 seconds using a gas mixture of carbon tetrafluoride (CF_4, 45 sccm). The remaining photoresist was removed by generously washing with acetone.

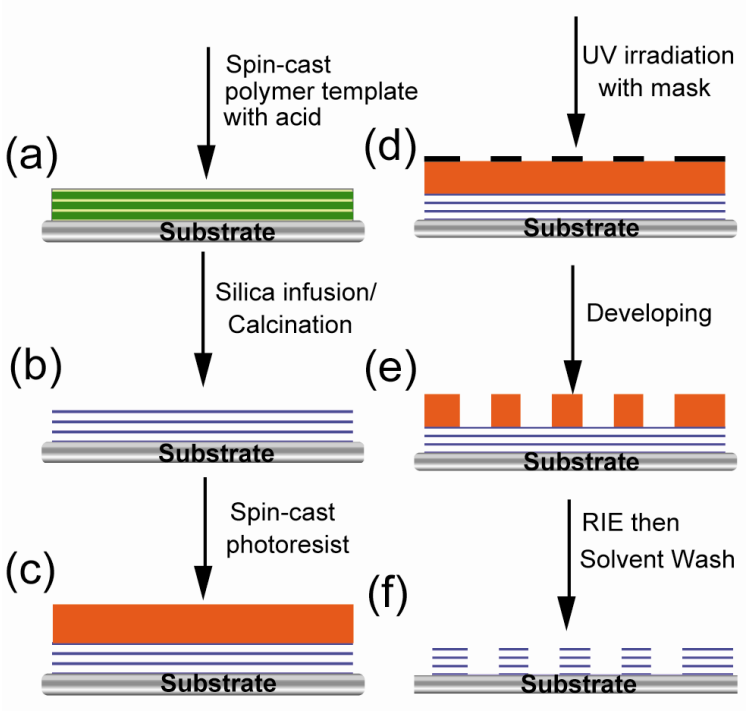

Figure 3.4: Device level patterning – Route 3. (a) A copolymer template is spun-cast with the appropriate homopolymer and pTSA. (b) Selective silica infusion into the polymer template and then calcined to yield a mesoporous silica film. (c) The sacrificial photoresist was spun cast on the resulting porous films, (d) followed by a UV exposure with a photomask to generate surface patterns. (e) Post development formed pillars of photoresist to protect the underlying mesoporous silica film (e). The patterned mesoporous silica is obtained through reactive ion etching followed by an acetone/isopropanol wash to remove any remaining photoresist.

3.3 Results and Discussion

Initial results using the UV lamp and TPST confirmed that acid diffusion is an extremely difficult problem to overcome even after introduction of the crosslinking agent TMMGU. The first series of route 2 exposed copolymers were replicated via the pre-heated method. Regardless of conditions, pattern replication was always poor (rough line edges) as shown using AFM in Figure 3.5. It is well-known that elevated temperatures increase diffusion rates. Therefore, minimal exposure to heat would be a distinct

advantage. As previously mentioned (Chapter 1), there are other thermodynamic paths open to reach the necessary reaction conditions. Pattern retention was significantly improved after employing the post-injection method. Once the silica condensation has begun the system should crosslink and prevent further acid diffusion. Figure 3.6 is an AFM of the resulting features. The line roughness has significantly improved but the pillars appear to be approximately 70-80 nm high while the surrounding matrix is around 30-40 nm. This implies that there is a thinner layer of silica that surrounds the pillars. The crosslinking was not ideal and requires optimization. Parameters to control would be the amount of TMMGU, UV dosage, heating time and temperature. The as-spun film was about 200 nm thick while the resulting silica film was less than 100 nm thick. Some shrinkage may occur during the calcination step but this large discrepancy occurs due to a lack of precursor, lack of generated acid or poorly controlled cross-linking.

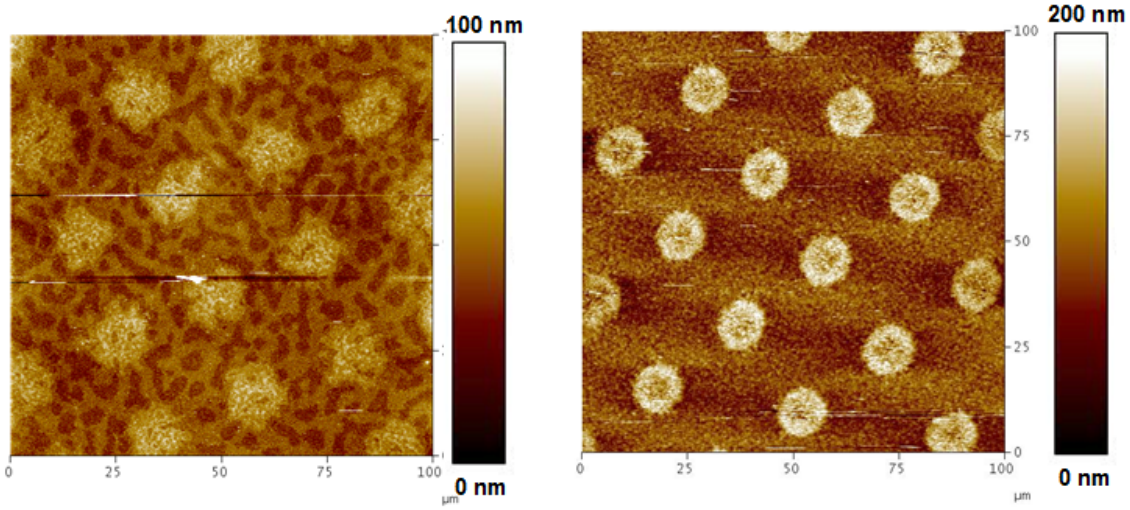

Figure 3.5: AFM images of mesoporous silica structures generated using a Pluronic F127 solution with TPST and TMMGU via Route 2 – Pre-heated procedure. A standard 254 nm UV Lamp and manual contact were used to pattern the substrates. The conditions were as follows: (Left) mask exposure 30 sec, 90 °C bake 40 sec, blanket exposure 30 secm (Right) mask exposure 60 sec, 90 °C bake 60 sec, blanket 60 sec. Note that the pattern improved but the edges remain rough.

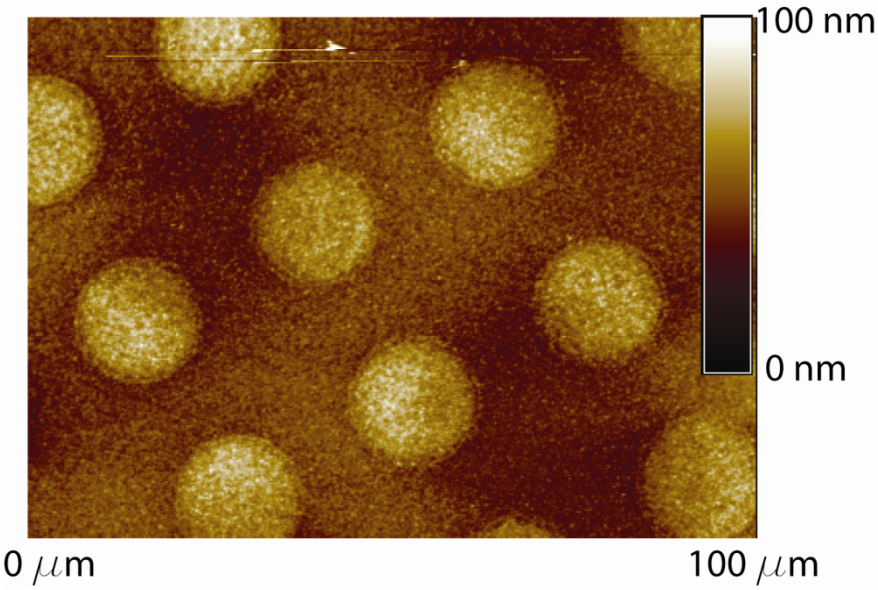

Figure 3.6: an AFM of mesoporous silica structures formed using the same route 2 and polymer solution as Figure 3.5. The difference is that the Pre-injection procedure was utilized to minimize exposure to heat and curb acid diffusion. The conditions were as follows: Mask exposure 30 sec, 90 °C bake 60 sec, blanket exposure 30 sec.

It became apparent that more rigorous lithography is required to reach smaller feature sizes. This can be accomplished with a specialized piece of equipment built for photolithography. A mask aligner offers controlled mask contact (vacuum or proximity) and has a narrower UV source. However, TPST is not active for the 365 nm lamp used by the available mask aligner, thus PAG121 (Ciba chemicals), an industrial available photoacid generator, was used for these experiments. The quartz photomask used for the following cases contained solid lines with width and spacing varying from 8 to 1 µm. Solutions consisted of Pluronic F127/20 wt% PHOST with 5 wt% PAG121 and 1 wt%

TMMGU when employing Route 2. They were spun-cast at 2000 RPM from solutions of 50/50 ethanol/ethyl acetate onto silicon substrates forming approximately 300 nm films. The films were each exposed for 3 minutes using low vacuum contact. The sample without TMMGU was infused as is while the sample containing crosslinker was heated at 90 °C for 30 seconds then flood exposed for another 3 minutes before infusion. Figure 10 compares results from each of the experiments. The first digit represents the linewidth (µm) while the second refers to the line spacing (µm) with respect to the original mask. Note the 1-1 section in each of the images. It is possible to resolve the line spacing in Figure 3.7 (right) while Figure 3.7 (left) appears almost as a single block. The crosslinking agent seems to be enabling small features with relatively small spacing. Route 1 generates a silica matrix with "holes" while Route 2 forms "tall" structures. The higher contrast seen in Figure 3.7 is the result an increased amount of silica from the matrix.

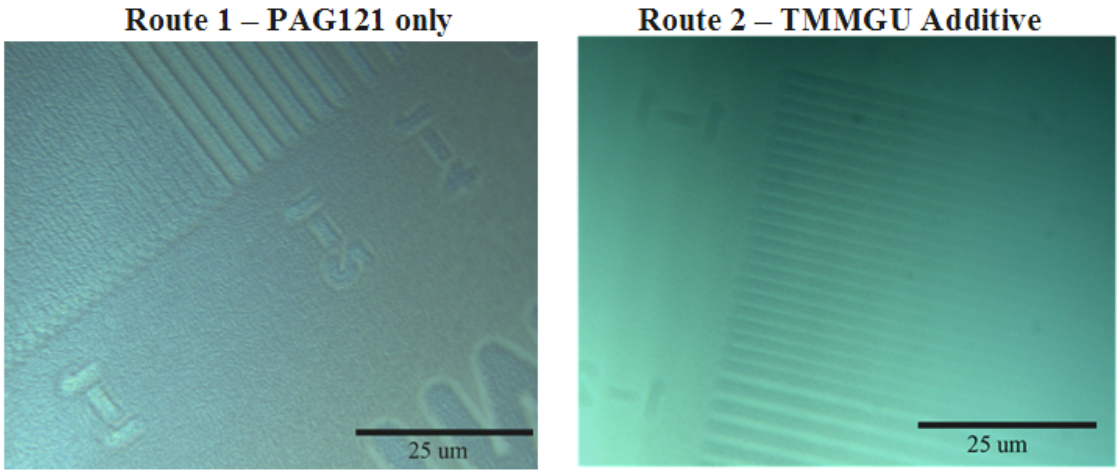

Figure 3.7: Optical micrographs of an array of lines obtained using (Left) Route 1 and (Right) Route 2 (crosslinking agent). The first digit refers to the line width (µm) while the second refers to the line spacing (µm). Notice that the line spacing cannot be indentified in the left image (1 µm - 1 µm) but addition of TMMGU via Route 2 enables more accurate pattern replication.

Route 3 (Figure 3.4) was developed in order to completely avoid the problem of acid diffusion. This method is based on conventional sacrificial photoresist optical lithography. Cylindrical mesoporous silica films were coated with a positive tone photoresist, exposed then developed to form a protective sacrificial pattern. The samples underwent reactive ion etching and then washed to form the porous structures. Figure 3.8 is an SEM of the resulting array. The discs are approximately 20 μm in diameter and 400 nm in height. The RIE conditions have not been optimized and the tapered edges seen in figure 3.8 are a result of this.

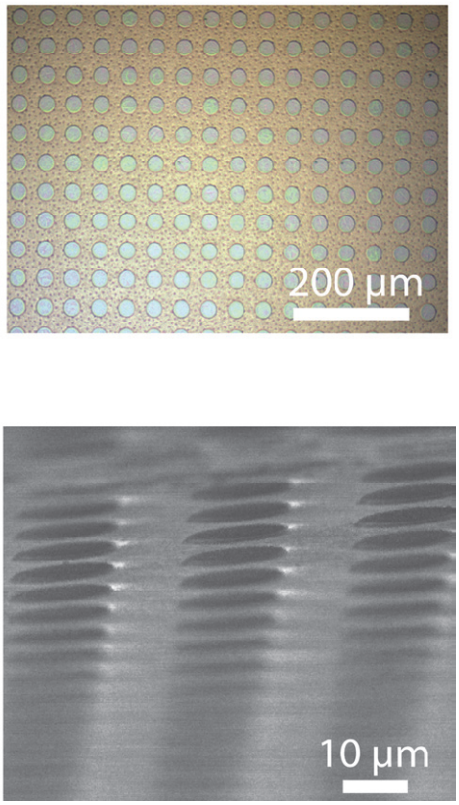

Figure 3.8: (Top) Optical micrograph showing the typical size scale and format of the samples. (Bottom) SEM micrograph of the mesoporous silica array prepared with a 15 second etch at 150 W and 100 mTorr with a flow rate of 45 sccm CF_4 and 5 sccm O_2.

3.4 Conclusions

Silica features with cylindrical pores parallel to the substrate were successfully developed. Supercritical CO_2 mediated silica condensation is compatible with a variety of optical lithography device fabrication techniques. It was shown that, although, difficult, it is possible to directly pattern Pluronic templated materials. The conditions have not been optimized but feasibility has been shown for Route 2. The problem of acid diffusion can be avoid altogether using route 3 but it can be difficult to attain straight edges when etching. Although further optimization is required for a true device the structures here are useful for further analysis of device feasibility as will be shown in later chapters. Structures that are one micron in length are approaching the current line width limitations for optical lithography at this campus. The next chapter utilizes nanoimprint lithography (NIL), another type of patterning technique that can reliably generate structures approximately 100 nm. Another distinct advantage of NIL is the incorporation into a roll-to-roll processing technique for inexpensive mass production.

3.5 References

(1) S. Nagarajan, J. K. Bosworth, C. K. Ober, T. P. Russell, J. J. Watkins, *Chemistry of Materials* **2008**, 20, 604-606.

(2) S. Nagarajan, T. P. Russell, J. J. Watkins, *Advanced Functional Materials* **2009**, 19, 1-7.

(3) D. Yang, S. W. Chang, C. K. Ober, *Journal of Materials Chemistry* **2006**, 16, 1693-1696.

(4) H. Jansen, H. Gardeniers, M. de Boer, M. Elwenspoek, J. Fluitman, *Journal of Micromechanics and Microengineering* **1996**, 6, 14-28.

CHAPTER 4

TOWARDS POROUS SILICA FILMS PATTERNED VIA NANOIMPRINT LITHOGRAPHY

4.1 Introduction

Nanoimprint lithography has two basic requirements – the first requirement being a mold with pre-made structures and the second being a suitable polymer or resist that will harden to retain structure and adhesive enough to not lift-off the substrate. A variety of polymers such as poly(benzyl methacylate) and poly(cyclohexyl acrylate) and UV curable resists have been patterned via NIL.[1] It is also possible to control polymer crystallization in films of poly(vinylidene fluoride) using NIL.[2]

Recently several groups have reported patterning substrates using the metal reflective film on polycarbonate discs from optical disc media of CDs and DVD's[3-5]. Control of patterned feature dimensions were realized through the appropriate selection of the optical disc media; either CD's, DVD's, HD-DVD's, and Blue-ray discs (~220nm, ~1,2μm), (~190nm, ~500nm), (~70nm, ~240nm), and (~20nm, ~180nm) (height, line width) respectively. Because of the low cost, readily available large active surface area, and submicron feature dimensions of these master molds, multiple reports of their use in micro- and nanopattering of spin-transition compounds[6], microtransfer molding (μTM)[7],and even role-to-role processing[8] have been reported. Most recently, DVD and CD patterned metal foils were removed and replicated with PVA flexible films and

incorporated into roll-to-roll processing.[8] Lal Das et al. reported a novel pattern miniaturization procedure, imprinting into swollen hydrogels of poly(acrylamide) using the CD and DVD metal film as the master mold[4].

Another well-known biocompatible hydrogel is poly(hydroxyethyl methacrylate) (PHEMA). PHEMA has been used in the literature as a readily removable lift of layer for lithographic patterning as well as a template for selective photolithographic cross-linking in the presence of a photo acid generator (PAG) and the acid sensitive cross-linking agent tetrakis(methoxymethyl) glycouracil (TMMGU). [9-11] The hydroxyl chemical functionality of PHEMA was utilized in this study to selectively functionalize imprinted PHEMA with SiO_2.

The first demonstration of the use of the polycarbonate molds of DVD's with nanoimprint lithography NIL to print into PHEMA was a result of this project. Pairing this printing technique with supercritical carbon dioxide mediated silica infusion enables high surface area replication involving metal oxides. After slight technique modifications it was shown that it is possible to infuse imprinted PHEMA without less of pattern.

However, block copolymers are significantly more interesting due to the inherent morphology associated with self-assembly. PDMS-b-PS copolymers were printed and utilized because of the O_2 etch contrast between a silicone based polymer and an organic polymer. [1, 12] Li *et al.* have utilized NIL of PS-PMMA in conjunction with thermal annealing to generate ordered domains within patterned areas.[13] Previous work has shown that PMMA-PHEMA doblock copolymers can form a variety of morphologies.[14] Therefore, the patterning/infusion technique developed within was also extended to PMMA-PHEMA diblock copolymers.

4.2 Experimental

4.2.1 Materials

Poly(2-hydroxyethyl methacrylate) (PHEMA) was synthesized by literature procedure (~10g). [9] The molecular weight ranged from 15k- 50k g/mol and had a glass transition temperature (Tg) of 78 °C. The diblock copolymer poly(methylmethacrylate)-Poly(2-hydroxyethyl methacrylate) (PMMA-PHEMA) was synthezised by atom transfer radical polymerization (ATRP) The total molecular weight was 21.4k g/mol where PHEMA is 70% by mass. All solvents, *para*-toleune sulfonic acid (pTSA), and low molecular weight poly(ethylene oxide) (PEO 1450 g/mol) were used as received from Sigma-Aldrich.

Master polycarbonate molds were generated by splitting the DVD/HD-DVD media disc then rinsing with an isopropyl alcohol (IPA)/ethanol mixture and finally dried under a nitrogen stream to remove the organic dye. In the case of PHEMA, the master molds were used without further modification. However, in the case of the diblock polycarbonate mold, approximately 10 nm of silicon monoxide (Kurt J. Lesker) was thermally deposited on the PC molds by using an Edwards Auto 306 Thermal Evaporator. Hydroxyl groups were created on the surface of the silicon monoxide layer on the PC molds by exposing the modified PC molds to an oxygen (O_2) plasma etch for 1 minute using a Harrick Scientific Plasma cleaner. To create a hydrophobic surface on the modified PC molds, the hydroxyl terminated PC molds were reacted with heptadecafluoro-1,1,2,2-tetrahydrodecyl-dimethyl chlorosilane through a vapor

deposition for 24 hours at 80°C. Prior to exposing the modified PC molds to O_2 plasma, a reactor was purged with N_2 for 1 hour prior to vapor deposition.

4.2.2 Procedure

4.2.2.1 Patterned PHEMA Film Preparation

A 3wt% (solids/total solution) solution of poly(hydroxyethyl methacrylate) (PHEMA) containing 0.1wt% poly(ethylene glycol) monomethylether (M_n = 2000g/mol) (PEO) and 0.2wt% p-toluene sulfonic acid monohydrate (pTSA) in ethanol (filtered through 0.45μm PTFE syringe filter) was spun-coat onto a (1.5 x 1.5 inch) silicon substrate at 3000 RPM for 20 seconds. The thin films (105 nm determined by profilmometry) were patterned with a freshly cleaned DVD-R polycarbonate mold using a NX2000 thermal imprinter with the following conditions: the pre-print was made at 50°C at 100 PSI for 30 seconds, printed at 90°C at 250 PSI for 30 s, cooled to 38°C and then the pressure was released. The printing procedure resulted in an accurate replication of the DVD-R polycarbonate disc into the PHEMA thin-film.

The general procedure for vapor infusing and cross-linking the PHEMA films with tetrachlorosilane (TCS) is detailed below. The patterned PHEMA wafers were placed on a glass pedestal in a I-CHEM jar (60mL) with a PTFE screw top and vacuum/backfilled 3x with N_2 followed by a 20min N_2 purge. Tetrachlorosilane (150 μL) was injected on the bottom of the jar then sealed with parafilm and left at room temperature for 12h. The patterned wafer was removed and analyzed.

4.2.2.2 Patterned PMMA-PHEMA Film Preparation

A 3 wt% (solids/total solution) solution of PMMA-b-PHEMA containing 0.1 wt% poly(ethylene glycol) monomethylether (M_n = 2000g/mol) (PEO) and 0.2 wt% p-toluene sulfonic acid monohydrate (pTSA) in ethanol (filtered through 0.45μm PTFE syringe filter) was spun-coat onto a 3.8 cm x 3.8 cm (1.5'' x 1.5'') silicon substrate at 3000 RPM for 20 seconds. The thin films (90 nm) were patterned with a freshly fluoronated (PC) mold using a NX2000 thermal imprinter with the following conditions: the pre-print was made at 50 °C at 100 psi for 30 seconds, printed at 130 °C at 250 PSI for 1 min, cooled to 38 °C and then the pressure was released. The printing procedure resulted in uniform negative replication of the fluorinated PC mold.

A general procedure cross-linking PMMA-b-PHEMA films with methyl trichlorosilane is described below. The polymer coated wafers were placed in a microwave vial and covered with 5 mL of toluene (anhydrous). Methyl trichlorosilane (0.25 mL, 5 v/v %) was added to the reactor via syringe and the reactor was sealed and heated at 90°C for 1 h, then cooled to room temperature. The wafer was washed in the vial with toluene (anhydrous) (3 x 10 mL) then removed and again washed extensively with toluene (anhydrous) to remove any un-reacted silane and dried under a stream of dry N_2.

4.2.2.3 Supercritical Fluid Mediated Infusion

The cross-linked patterned films were replicated with silica via a supercritical carbon dioxide ($scCO_2$) mediated silica condensation. After lightly cross-linking, the

substrate was placed in a 140 mL stainless steel high-pressure reactor at room temperate with 25-50 μL of water and approximately 5 μL tetraethylorthosilicate (TEOS) per cm^2 of patterned substrate. Approximately 35 mL of carbon dioxide (Airgas East Bone-dry grade) at 69 bar (~1000 psi) and room temperature was injected into the sealed reactor via a syringe pump within 20 min. Immediately after injection, the wall temperature was heated to 220 °C which brought the gas to a temperature of 160 °C over 2 hr while increasing the pressure to 120 bar (~1800 psi). The system was allowed to react at the maximum pressure and temperature for at least 12 hours then depressurized over 20 min. The organic PHEMA template was then removed through calcination at 400 °C for 6 hr with a ramp rate of 1.67 °C/min.

4.3 Results and Discussion

Silica replicates of patterned PHEMA and PMMA-PHEMA were successfully generated with little height loss. All of the patterns were created with inexpensive and readily available DVD and HD-DVD polycarbonate molds which yielded patterns that are submicron in all dimensions. Initially, the nanoimprint lithography (NIL) procedure was attempted with Pluronic systems. However, regardless of master mold fluorination, the surfactant systems would adhere to the mold itself and lift-off from the substrate producing poor patterns. Thus other systems were examined.

4.3.1 PHEMA

Thin PHEMA films (200-300 nm) were spun onto O_2 cleaned silicon substrates then patterned using nanoimprint lithography. A small amount of PEO was incorporated into the mixture to act as a plasticizer and decrease the Tg while pTSA was also added as an acid catalyst for the silica condensation step. PEO enabled lower printing temperatures and more complete mold filling. A schematic for this process is showed in Figure 4.1.

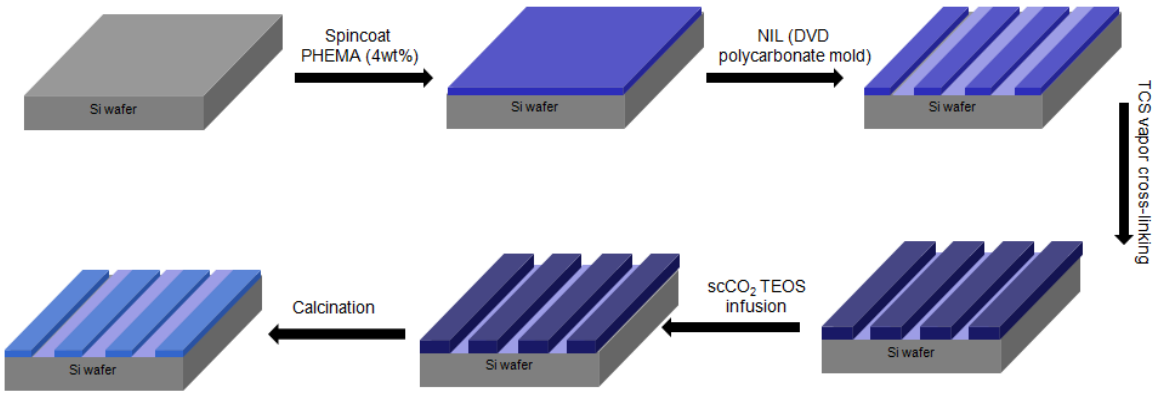

Figure 4.1: Schematic of the NIL – $scCO_2$ infusion process for the PHEMA template.

The DVD master mold had original dimensions of (~190 nm height with lines ~500 nm with a periodicity of ~800 nm). The print would be the negative of the DVD mold thus the DVD trenches should match the printed peak heights. However, this is not the case due to inaccurate height AFM measurements resulting from static charge on the polycarbonate mold. Nevertheless, the width can be used to gauge the completeness of the print. Smaller peak widths would imply incomplete prints.

PHEMA hydrophilicity both helped and hindered the processing of the patterned substrates. The hydrophilicity of the PHEMA thin-film simplified the NIL printing procedure by allowing the use for DVD polycarbonate disc without any further modification. Furthermore, the sample preparation required great care in preventing adsorption of ambient water, which readily reacts with chlorosilanes used as the cross-linking agent in the next step. This adverse reaction was limited by storing each sample directly after imprinting in a desiccator. The inherent chemical functionality of PHEMA was utilized in the further functionalization of the patterns through TEOS infusion.

Patterned Sample	TEOS	Wall Temp (°C)	Stage Temp (°C)	Gas Temp (°C)	CO_2/Soak	Post-Infuse	Calcine
PHEMA/PEO	7 μL	65	N/A	40	120mL/1hr	Pattern	None
PHEMA	7 μL	65	N/A	40	120mL/1hr	Pattern	None
PHEMA/PEO	7 μL	45	45	40	120mL/1hr	Pattern	None
PHEMA	7 μL	45	45	40	120mL/1hr	Pattern	None
PHEMA/PEO	7 μL	120	N/A	90	60mL/1hr	None	Silica
PHEMA	7 μL	120	N/A	90	60mL/1hr	None	Silica

Table 4.1: Reaction schemes completed without pre-crosslinking with chlorosilane. The substrate size was approximately a 1.27 cm (0.5'') by 1.27 cm (0.5'') wafer. Note that it was impossible to both retain pattern and infuse the sample simultaneously. The infusion process is completed over Tg but the sample begins to flow at elevated temperatures.

Initially the $scCO_2$ procedure was attempted on samples immediately after printing without any further modification. The glass transition temperature of bulk PHEMA is approximately 75 °C. As seen in Table 4.1, samples reacted under this threshold temperature retained their patterns after infusion but when calcined there was nothing left on the surface of the wafer. The supercritical carbon dioxide did not swell the polymer enough to enable a degree of condensation that the structure would be self standing after removal of the organic template. Reactions completed over Tg result in a

stable silica film but without the pattern. Above the Tg (and during CO_2 swelling) the sample flows and the pattern is lost. These competing mechanisms completely prevent replication.

Patterned Sample	TEOS	Wall °C	Stage °C	Gas °C	CO_2/Soak	Post-Infuse	Calcine
PHEMA/PEO (CL)	15 μL	90	90	75	60mL/1hr	Pattern	Shallow
PHEMA (CL)	15 μL	90	90	75	60mL/1hr	Pattern	Shallow
PHEMA/PEO	15 μL	90	90	75	60mL/1hr	Pattern	None
PHEMA	15 μL	90	90	75	60mL/1hr	Pattern	None
PHEMA/PEO (CL)	15 μL	150	N/A	110	45mL/1hr	Pattern	Shallow
PHEMA (CL)	15 μL	150	N/A	110	45mL/1hr	Pattern	Shallow
PHEMA/PEO (CL)	30 μL	230	N/A	165	35mL/2hr	Pattern	Increase
PHEMA (CL)	30 μL	230	N/A	165	35mL/2hr	Pattern	Increase

Table 4.2: Reaction schemes completed after pre-crosslinking with chlorosilane (CL). Again the sample size was approximately a 1.27 cm (0.5'') by 1.27 cm (0.5'') wafer. All of the reactions with crosslinking were completed above or at Tg and retained the pattern. However, after calcination pattern height was lost.

It was determined that, with the elevated temperatures needed for the complete SiO_2 infusion of the patterned substrates, a chemical cross-linking reaction was required. Slightly crosslinking the samples with a chlorosilane prevented the pattern from flowing so that the infusion could occur above the Tg. Table 4.2 displays reaction conditions and compares the results of crosslinked (CL) films to unmodified. All of the reactions were completed at or above Tg. Even though it was possible to form silica replicates of the patterns, these patterns were less than half of the original height. AFM images of samples that underwent the 230 °C wall temperature with a 2 hour soak time are shown in Figures 4.2 and 4.3. Figure 4.2 displays ridges that were a result of poor printing conditions. Although technically a mistake, this shows that the $scCO_2$ process can be

utilized for any type of arbitrarty geometry. Figure 4.3 shows an HD-DVD patterned film under the same high temperature/short soak time conditions. Note that most of the height was also lost in this case. The AFM artifacts that occur after the crosslinking step occur when the PHEMA is not kept under a desiccator and allowed to adsorb too much water. In order to promote further condensation, the reaction time was extended to an overnight soak. Table 4.3 displays the conditions examined. The best results were attained well above the T_g and these became the conditions for all further reactions.

Patterned Sample	**TEOS**	**Wall °C**	**Stage °C**	**Gas °C**	**CO2/Soak**	**Silica (calcine)**	**Pattern (calcine)**
PHEMA/CL	15 μL	90	90	72	Overnight	No	No
PHEMA	15 μL	90	90	72	Overnight	Yes	Shallow
PHEMA/PEO/CL	15 μL	90	90	72	Overnight	No	No
PHEMA/PEO	15 μL	90	90	72	Overnight	Yes	No
*PHEMA/CL	15 μL	230	N/A	165	Overnight	*Yes	*Yes
PHEMA	15 μL	230	N/A	165	Overnight	Yes	No
*PHEMA/PEO/CL	15 μL	230	N/A	165	Overnight	*Yes	*Yes
PHEMA/PEO	15 μL	230	N/A	165	Overnight	Yes	No

Table 4.3: Samples were allowed to soak overnight. Again the sample size was approximately a 0.5'' by 0.5'' wafer. The higher temperature cases retained almost full pattern height. The height lost was due to normal shrinkage that occurs during calcincation. Samples denoted with asterisks (*) were successful replications.

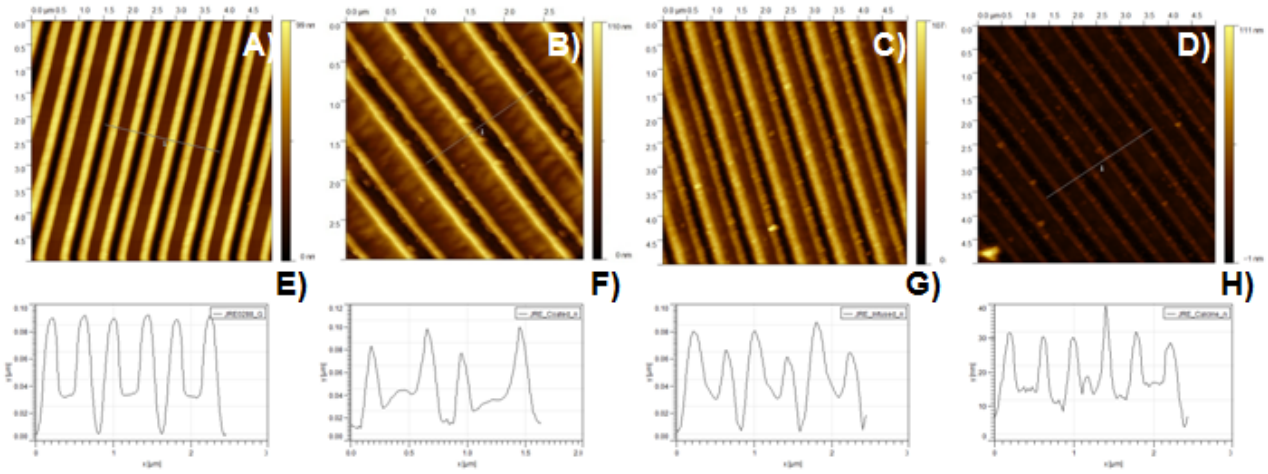

Figure 4.2: All AFM images reported are 5x5µm topographic images: A) Image of NIL patterned PHEMA 140nm thinfilm, B) Image of TCS crosslinked patterned PHEMA film C) Image of scCO2 Infused sample D) Image of the calcined silica thin film. Images E) through H) are tracer profile plots from the topographic images A) through D) respectively. The non-optimized patterning conditions did not accuratly replicate the mold. Furthermore, due to the reaction conditions, after calcination there is a large amount of height loss.

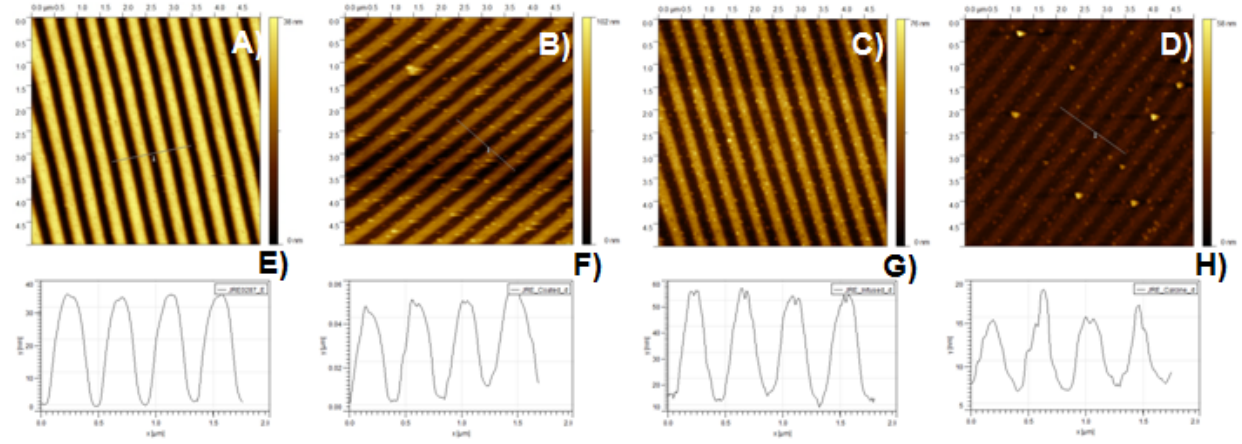

Figure 4.3: All AFM images reported are 5x5µm topographic images: A) Image of NIL patterned PHEMA 140 nm thin film, B) Image of TCS crosslinked patterned PHEMA film C) Image of scCO2 Infused sample D) Image of the calcined silica thin film. Images E) through H) are tracer profile plots from the topographic images A) through D) respectively. The HD-DVD mold was successfully replicated but height loss remains an issue.

The sample in Figure 4.4 was characterized throughout this process by ATR-FTIR and water contact angle to offer insight into this new process. Table 4.4 organizes the measurements from AFM at each step of the process. The contact angles of TCS cross-linked patterns (0°) did not change from those measured with spin-coated PHEMA (0°). Both patterned and smooth thin-film samples adsorbed the water droplet before a measurement could be performed. In order to insure complete chemical cross-linking of the PHEMA substrates a test sample was washed with copious amounts of methanol without an observable change. Interesting results in the ATR-FTIR spectra (Figure 4.5) confirmed a chemical change in the film with a decrease in the magnitude of the carbonyl vibrational stretch 1725 cm^{-1} ν(-C=O) and a dramatic increase in the peaks 1300-1000 cm^{-1} characteristic of ν(Si-O) and ν(C-O) stretching vibrations.[15] After the TCS chemical cross-linking, an intense peak appeared at 933 cm^{-1} ν(Si-OH), which corresponds to a silanol vibrational stretch. A characteristic broad peak 3600-3000 cm^{-1} ν(O-H) was evident in both the PHEMA and TCS cross-linked thin-films which represents a combination of the silanol and hydroxyl group on PHEMA and infused TCS as well as ambient adsorbed water in the thin-film. A slight increase in the width (~30 nm) and height (~5 nm) of the patterned lines was observed in the AFM images. This was a direct result of the chlorosilane swelling of the polymer film. Condensation of the silianol functionality in the film was limited in the cross-linking step with the room temperature reaction conditions, which was thought to improve the infusion of TEOS in the thin-film through only light cross-linking. A similar process was performed with photochemical cross-linking of PHEMA-b-PAA with an acid sensitive cross-linker TMMGU in which solution based infusion was performed on micro-scale patterns

resulting in the formation of SiO_2 nanoparticles. This cross-linking procedure was attempted with thermal NIL of our PHEMA films, which resulted in cross- linked films before complete imprinting could be performed. [11]

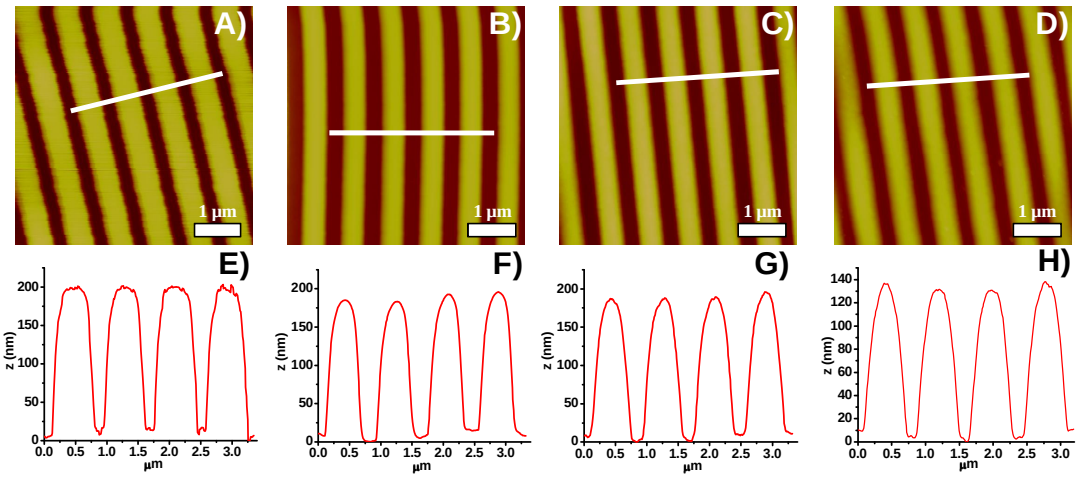

Figure 4.4: All AFM images reported are 5x5µm topographic images: A) Image of DVD-R polycarbonate master mold, B) Image of NIL patterned PHEMA 140nm thinfilm, C) Image of TCS crosslinked patterned PHEMA film, D) Image of scCO2 TEOS infused thin film followed by calcinations. Images E) through H) are tracer profile plots from the topographic images A) through D) respectively.

Sample	Height (nm)	Plateau width (nm)	Periodicity (nm)
DVD master mold	187.5±0.57	507.4±8.5	808.8±8.1
PHEMA patterned	179.0±2.5	450.0±2.9	816.5±5.9
TCS (vapor) crosslinked	183.6±3.9	484.4±2.9	822.7±4.1
$scCO_2$ infused	175±3.7	481.8±6.4	786.8±11.1
calcined	129.5±0.5	443.7±4.9	759.1±5.9

Table 4.4: Height measurements from Figure 4.4

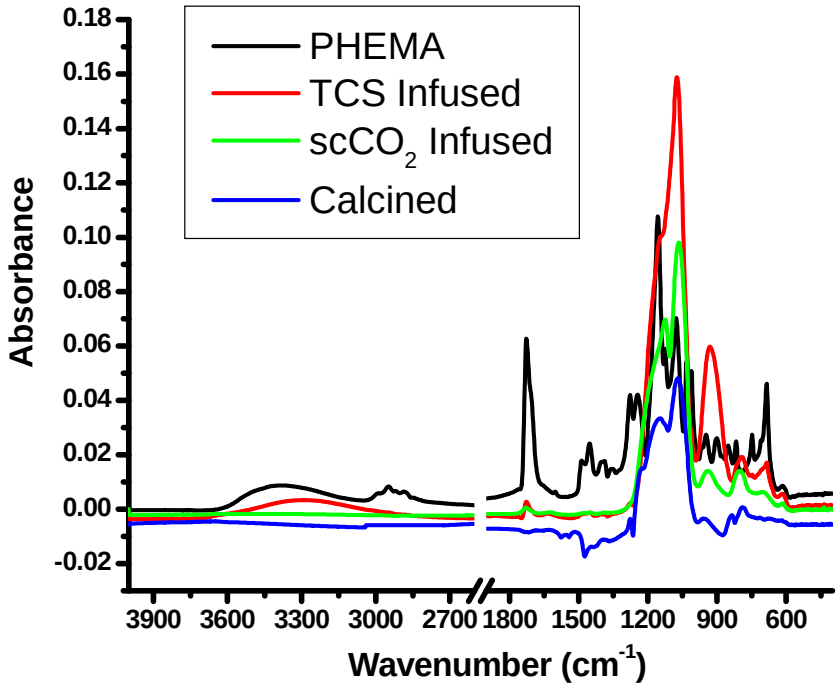

Figure 4.5: ATR-FTIR spectra of a PHEMA thin-film pre-treated, exposed to TCS vapors for 12 h, $scCO_2$ infused with TEOS (5 µL/cm^2) for 12 h at 160 °C, and calcined at 400 °C for 6 h.

A control experiment was performed with the calcinations of a patterned substrate omitting the $scCO_2$ infusion step, which resulted in little to no pattern retention. After the infusion step, the contact angle remained 0°, again adsorbing in the film. The disappearance of peaks from 1500-1300cm^{-1} characteristic $\delta(CH_2,CH_3)$ respectively in the FTIR spectra was not expected after infusion because the T_g measured by DSC was 400°C. Not only was the heating time extended to that of the DSC but it is also believed the addition of pTSA to catalyze the condensation of TEOS in the PHEMA film as well as acid incorporated in the cross-linking step decreased the degradation temperature of PHEMA through acid hydroylis.[16]

After calcincation, small changes in the intensity of the FTIR spectra were observed but no appearance/disappearance of any additional peaks. A decrease in the

height features by (~50 nm) was observed with an equivalent decrease in the line width (~440 nm) and periodicity (~760 nm). This decrease in the pattern dimension is a result of further condensation of the infused SiO_2 commonly reported in $scCO_2$ infusions a result of the dilatation of the polymer film with $scCO_2$. No change in the contact angle throughout the creation of these patterned SiO_2 lines was observed.

4.3.2 PMMA-PHEMA

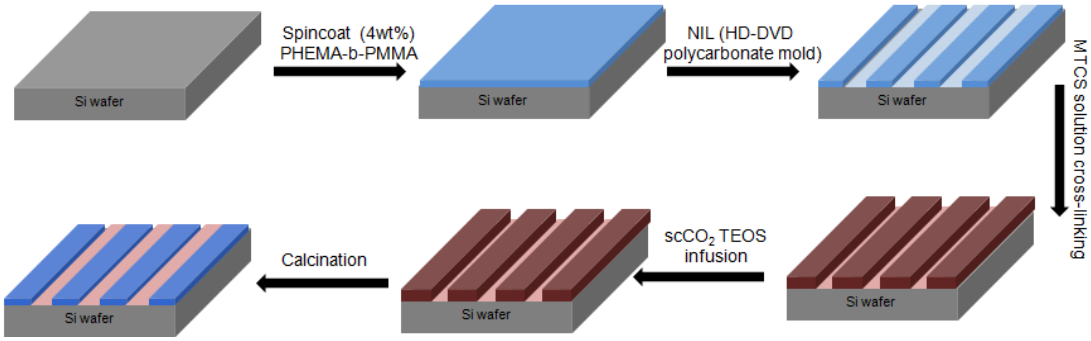

Figure 4.6: Schematic of the NIL – scCO2 infusion process for the PHEMA-PMMA copolymer template.

This process was then expanded to diblock copolymers. PMMA-PHEMA has been previously shown to order and seemed a likely extension to the previous PHEMA work.[14] The crosslinking procedure was slightly different from the one used previously (described in section 4.2.2.2) and prevented formation of silica particles on the patterned samples. The supercritical carbon dioxide mediated infusion and the subsequent calcination remained similar to the procedure for the PHEMA template. A schematic is shown in Figure 4.6.

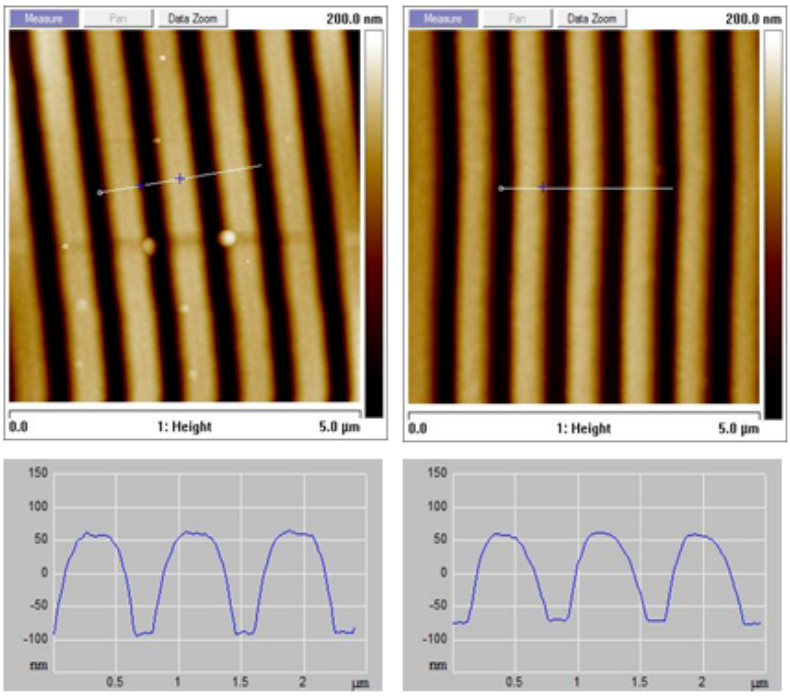

Figure 4.7: Examples of replicated PHEMA-PMMA templates. The left image is post-infusion while the right image is post calcination. The results are similar to that of the PHEMA only case.

Figure 4.7 shows infused and calcined AFM images using PMMA-PHEMA diblock copolymer. These structures have an inherent porosity due to the silica condensation only occurring within the PHEMA block. However, these samples are only porous and not yet well-ordered. Figure 4.8 shows an SEM of calcined silica prepared using a PMMA-PHEMA template along a TEM displaying the porous nature of material. There are many options available to order these diblock copolymers including thermal annealing, solvent annealing and even ordering using NIL itself.[13]

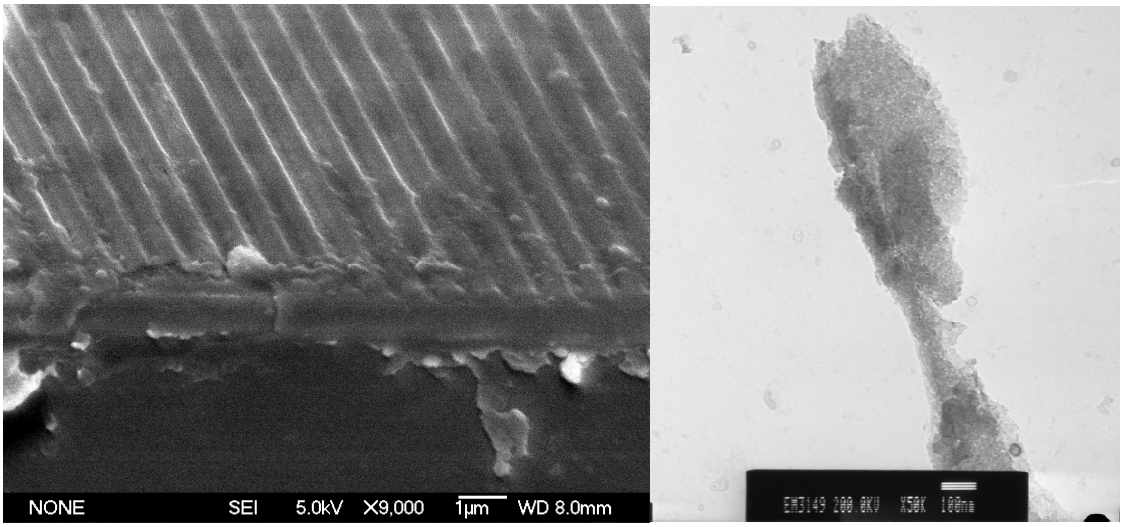

Figure 4.8: SEM (left) and TEM (right) micrographs of DVD patterned calcined silica using PMMA-PHEMA as the template. The particles along the edge are a result of the sample fracturing step. The materials are porous but lack a well-ordered structure.

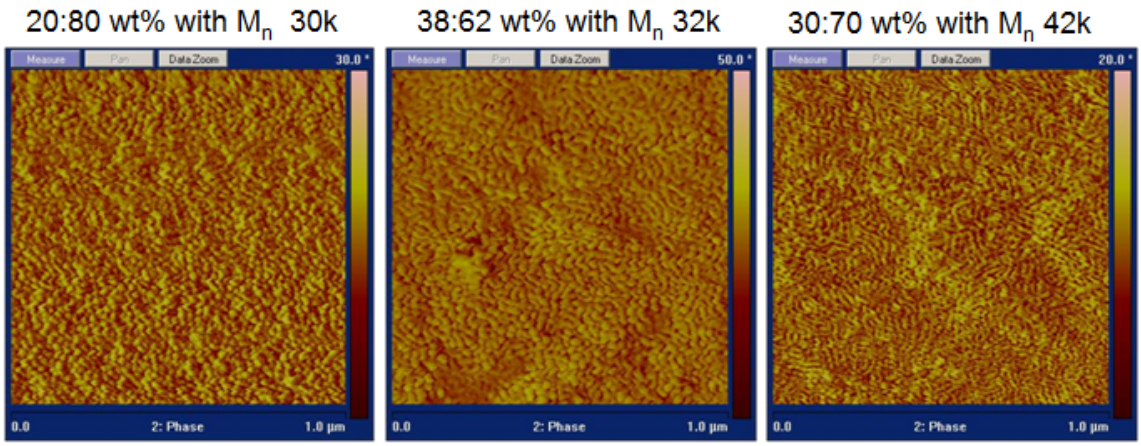

Figure 4.9: AFM of three molecular weight ratios of ordered PMMA-b-PHEMA 50 nm films (0.5 wt% solution, 1000 RPM). PHEMA is the greater percentage in each of the diblocks. Each film was spun from methanol then annealed in MeOH for 17 hours.

Three molecular weight ratios were printed and replicated using this process. Although the samples have not yet been well-ordered after the print, preliminary results show that these copolymers can order. Figure 4.9 displays phase AFM images that show three types of morphology. Each sample was annealed in a methanol vapor for 17 hours. Methanol is a good solvent for both of the blocks. The left most image corresponds to a molecular weight ratio of PMMA-PHEMA 20:80 wt% with a total Mn of 30k g/mol and displays a morphology that's resembles spheres. The center image has a ratio of PMMA-PHEMA 38:62 wt% with a total Mn of 32k g/mol and appears to be lamellar. The third right-most image has a ratio of PMMA-PHEMA 30:70 wt% with a total Mn of 42k g/mol and has a cylindrical morphology parallel to the substrate.

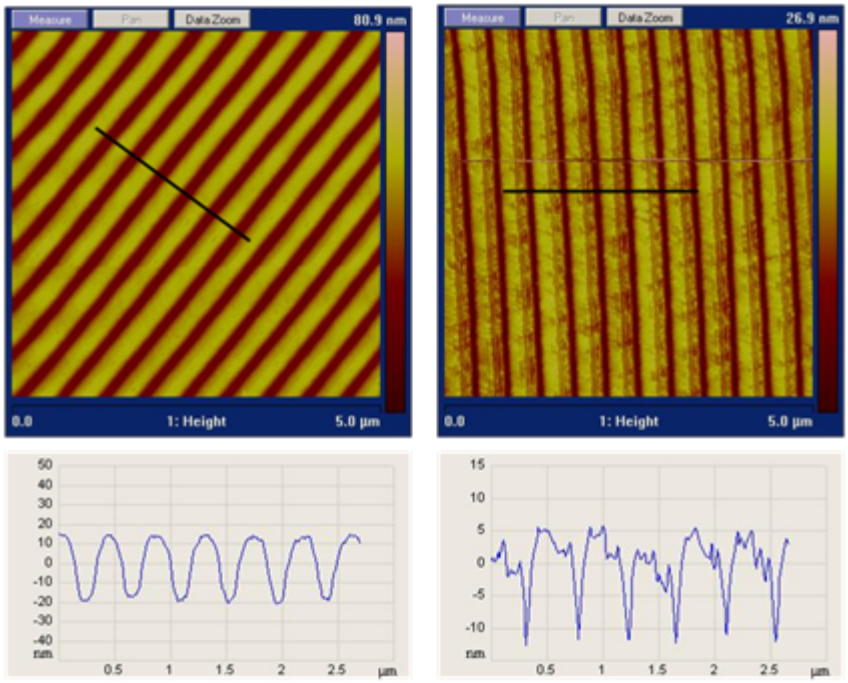

Figure 4.10: Comparison between $scCO_2$ mediated silica infusion (left) and vapor phase silica infusion (right). The $scCO_2$ process is neccesary to maintain structure fidelity.

A comparison between calcined samples of the cross-linked then $scCO_2$ infused with that of a sample that has only been cross-linked is shown in Figure 4.10. The infused sample completely retains the pattern while the cross-linked only is no longer a rigid and complete structure. This reinforces the importance of the infusion step

4.4 Conclusions

Nanoimprint lithography enables smaller patterned features of arbitrary geometries than those created in previous chapters by optical lithography. NIL also has the advantage of being able to be implemented in a roll-to-roll processing procedure. In this chapter, NIL followed by $scCO_2$ mediated TEOS infusion was successfully utilized to generate mesoporous silica patterns of an arbitrary geometry. However, the NIL process did not work with Pluronic® systems due to poor substrate adhesion. It may be possible to remedy this solution through other means of substrate and mold modification. Instead PHEMA and PMMA-PHEMA diblock copolymers were utilized. In order to retain pattern rigidity the patterns were pre-crosslinked through either a vapor phase or solution phase chlorosilane reaction. The $scCO_2$ process was modified to infuse these crosslinked polymers so that there would be no loss of pattern height. Mesoporous silica patterns were generated but they were not well-ordered. As shown here and in literature, there is potential to order these polymers but more research is required for control of the order in these patterned then replicated materials.

4.5 References

(1) L. J. Guo, *Advanced Materials* **2007**, 19, 495-513.

(2) Z. Hu, G. Baralia, V. Bayot, J.-F. Gohy, A. M. Jonas, *Nano Letters* **2005**, 5, 1738-1743.

(3) M. S. V. B. Heinz Mustroph, *Angewandte Chemie International Edition* **2006**, 45, 2016-2035.

(4) R. M. V. K. M. K. A. G. A. S. A. Lal Das, *Advanced Materials* **2007**, 19, 1943-1946.

(5) K. Youngmin, B. Jaecheol, K. Hongmin, K. Shinill, *Journal of Physics D: Applied Physics* **2004**, 1319.

(6) I. B. S. M. G. R. I. S. Z.-R. Q. R. C. M. R. Massimiliano Cavallini, *Angewandte Chemie International Edition* **2008**, 47, 8596-8600.

(7) L.-Y. Hong, D.-H. Lee, D.-P. Kim, *Journal of Physics and Chemistry of Solids* **2008**, 69, 1436-1438.

(8) R. Mukherjee, A. Sharma, G. Patil, D. Faruqui, P. Sarathi, G. Pattader, *Bulletin of Materials Science* **2008**, 31, 249-261.

(9) I. W. Moran, D. F. Cheng, S. B. Jhaveri, K. R. Carter, *Soft Matter* **2008**, 4, 168-176.

(10) I. W. Moran, A. L. Briseno, S. Loser, K. R. Carter, *Chemistry of Materials* **2008**, 20, 4595-4601.

(11) J. Ford, S. Yang, *Chemistry of Materials* **2007**, 19, 5570-5575.

(12) C. Y. Hua, A. Jagota, Y. Y. Lin, E. J. Kramer, *Langmuir* **2002**, 18, 1394.

(13) H.-W. Li, W. T. S. Huck, *Nano Letters* **2004**, 4, 1633-1636.

(14) D. Yin, S. Horiuchi, T. Masuoka, *Chemistry of Materials* **2005**, 17, 463-469.

(15) E. Pretsch, Bühlmann, Philippe, Badertscher, Martin *Structure Determination of Organic Compounds*. 4th ed. ed. Tables of Spectral Data 2009: Springer Berlin Heidelberg. 436 p. 491 illus.Softcover.

(16) I. G. M. V. G. M. G. M. Gurruchaga, *Journal of Applied Polymer Science* **1993**, 47, 1003-1011.

CHAPTER 5

UTILIZATION OF MULTI-SCALE DEVICES FOR SELECTIVE SEGREGATION OF GOLD NANOPARTICLES

5.1 Introduction

Mesoporous silica structures are currently being examined for applications such as sensors[1] and nanofluidics[2]. Yamaguhci *et al.* have used porous structures to sepeparate different sized biomolecules.). It was shown the device with 3.4 nm channel diameter successfully excluded myoglobin (~4.0 nm) and bovine serum albumin (BSA, ~7.2 nm) but allowed rhodamine B (~1 nm) and vitamin B12 (~2.4 nm) to pass through[3]. Control of the mesostructure morphology and size would be beneficial for any type of sensing or separation device. Rhodamine dye is a positively charged hydrophilic dye that diffuse into the porous silica material. It has been shown that the dye is stable within silica structures (more stable than in water) and can be used as a fluorescent tag.[4-6] It is also known that gold nanoparticles can quench or enhance fluorescence depending on size of the particles and distance to the fluorophore.[7] Therefore, the devices developed within the previous chapters were immersed in rhodamine dye followed by immersion in gold nanoparticle solutions of difference sizes and their feasibility examined.

5.2 Experimental

5.2.1 Materials

All chemicals, except the following reagents, are purchased from Sigma-Aldrich Inc. and used as received without further purification. Triblock copolymers of poly(ethylene oxide)$_{106}$-poly(propylene oxide)$_{70}$-poly(ethylene oxide)$_{106}$ (Pluronic F127) and poly(ethylene oxide)$_{127}$-poly(propylene oxide)$_{48}$-poly(ethylene oxide)$_{127}$ (Pluronic F108) are obtained from BASF. The photoresist, S1813, and Developer 351 are purchased from Rohm and Haas Electronic Materials. The silicon wafer was obtained from University Wafer. Rhodamine 6G Dye is has an approximate diameter of 1.34 nm with an excitation wavelength of 520 nm and an emission wavelength of 553 nm. Water soluble gold nanoparticles (GNPs) were synthesized in-house using various techniques described below.

5.2.2 Procedure

5.2.2.1 Preparation of Mesoporous Silica Thin Films

A polymer blend of amphiphilic block copolymers of Pluronic F127 or Pluronic F108 with 20 wt% poly(acrylic acid) (PAA, M_w = 1800) were used as templates for generating mesoporous silica films. A solution of Pluronic/PAA with 5 wt% p-toluenesulfonic acid (pTSA) in a mixture of ethanol/water (v/v = 50/50) were spun-coat onto 50.8 mm diameter silicon substrates. The spinning rate and time were

maintained at 2000 rpm and 60 sec to yield a polymer film with an approximate thickness of 400-500 nm. The substrate was placed in a high-pressure reactor with a few drops of water and annealed at 60 °C for 10 min. After annealing (pre-heating method), the silica precursor, tetraethyl orthosilicate (TEOS, 7 µL) was introduced into the reactor, followed by injection of $scCO_2$ (Merriam Graves Coleman grade) at 60 °C and 124 bar. The reactor was pressurized over 1.5 hr, held at the final conditions for 30 min, and depressurized slowly overnight. The organic templates were removed through calcination at 400 °C for 6 hr with a ramp rate of 1.67 °C/min to obtain a smooth mesoporous silica film.

5.2.2.2 Patterning of Mesoporous Silica Thin Films

Route 3 (Chapter 3) was used to generate the devices. The positive tone photoresist (S1813) was spun onto the mesoporous silica films at 3000 rpm for 30 sec and baked at 100 °C for 75 sec. The substrate was then exposed with UV light (350 w Hg lamp, 20 watts/cm^2) at 365 nm for 4.5 sec using a mask aligner (SUSS Microtec) with low vacuum contact. A quartz mask with 25 µm opaque circles was used for the patterning. After irradiation, the samples were developed using a mixture of water/Developer 351 (v/v = 4:1) yielding pillars with a height of 1.5 µm. Reactive ion etching (RIE, Trion) was completed at 100 mTorr with an RIE setting of 150 watts using a gas mixture of carbon tetrafluoride (CF_4) (45 sccm) and oxygen (5 sccm) between 5 and 40 sec. The remaining photoresist was removed by washing with acetone.

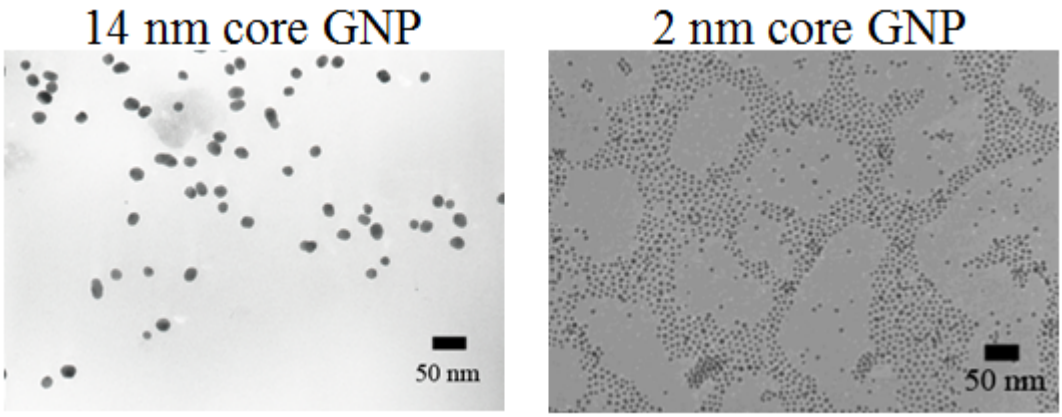

Figure 5.1: (Left) 14 nm Core GNP with a particle size range of 13 – 15 nm. (Right) 2 nm Core GNP with a particle size ranging from 2 – 4 nm.

5.2.2.3 Gold Nanoparticle Synthesis

The gold nanoparticles with 14 nm core (GNP-14 nm) were synthesized according to the reported procedure.[8] The small gold nanopaticle with diameter of 2 nm was prepared based on the published method, followed by place-exchange with 6-mercapto-N,N,N-trimethtyl hexane-1-ammonium to yield a water soluble cationic gold nanoparticle (GNP-2 nm).[9] Each set of particles was prepared Hung-Ting Chen and Myoung-Hwan Park who are advised by Proffesor Rotello (Chemistry – University of Massachusetts). TEM micrographs of each type of gold nanoparticle are shown in Figure 5.1.

5.2.2.4 Infusion of Rhodamine 6G Dye

A patterned mesoporous silica film, prepared from RIE for 20 sec, was placed in an aqueous solution of Rhodamine 6G (0.1 μM, $\varepsilon_{260\ nm} = 8.02\times10^4\ M^{-1}cm^{-1}$) for 5 min, followed by washing with copious amount of water and ethanol, then dried with N_2 gas. The resulting dye-uptake silica film was subjected to study by fluorescence microscopy and confocal laser scanning microscopy.

5.2.2.5 Quenching Fluorescence of Dye Solutions with Gold Nanoparticles

The fluorescence of Rhodamine 6G dye (0.1 μM) was quenched with either 2 nm or 14 nm gold nanoparticles at various concentrations and observed with excitation wavelength at 500 nm. The normalized concentrations are shown in Figure 5.2

Dye up-taken mesoporous silica patterns were prepared at 0.1 μM solution of Rhodamine 6G. Concentrations of individual gold nanoparticles were chosen based on aforementioned quenching study in solution (GNP-14 nm = 2.37 nM and GNP-2 nm = 16.0 μM). The patterned silica film was split and immersed in each gold nanoparticle solution for the same amount of time. The fluorescence intensity of silica patterns after quenching by gold nanoparticles was observed by fluorescence microscopy.

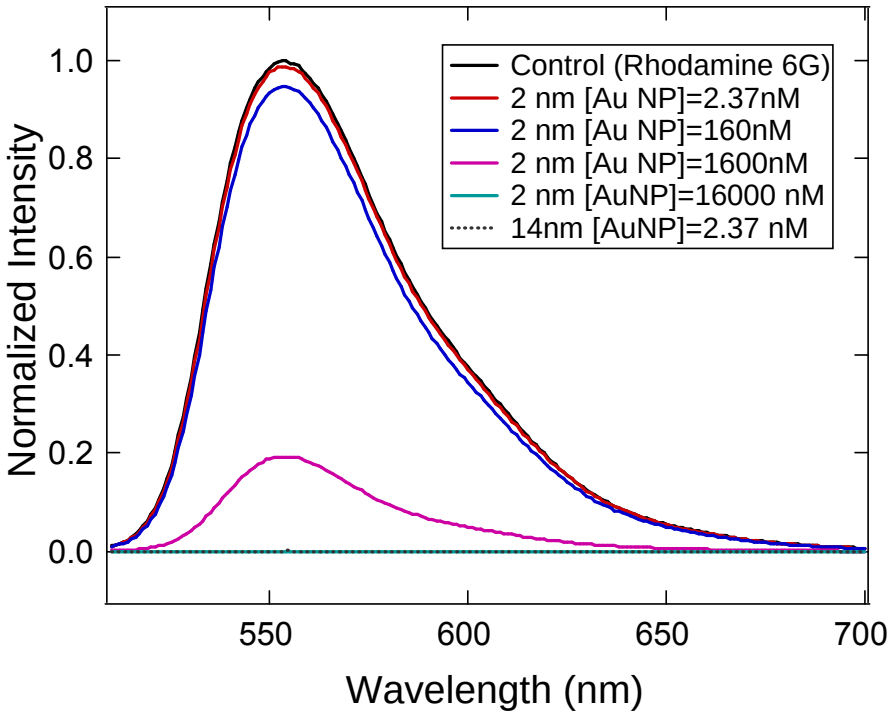

Figure 5.2: Normalized emission spectra of various dye solutions measured using fluorescence spectroscopy with excitation wavelength at 500 nm. (a) 0.1 μM Rhodamine 6G (b) with 2.37 nM GNP-2 nm (c) with 1.6 μM GNP-2 nm, (d) with 16 μM GNP-2 nm, and (e) mixture of 0.1 μM Rhodamine 6G and GNP-14 nm at 2.37 nM.

5.3 Results and Discussion

The accessibility of mesochannels in regular circular patterns was examined by impregnation of fluorescent dye within the mesoporous silica films and the schematic for this process is shown in Figure 5.3. In this study, we specifically chose a positively charged Rhodamine-6G dye with a diameter of 1.34 nm, which should diffuse into the channel and absorb on the silica framework through complementary electrostatic interaction. The confocal laser scanning microscopy (LSM) image of Rhodamine-6G infused mesoporous silica film exhibits an array of green fluorescent

dots with feature size of approximately 20 μm. This corresponds to the size of lithographically patterned silica domains (Figure 5.4). The dark background indicates that no nonspecific adsorption occurred between the Rhodamine 6G dye and silica surface. The result demonstrated accessibility of mesoporous structures in the patterned silica matrix after the photolithographic process. The accessibility of mesochannels originated from a reduced diffusion pathway due to the miniaturization of silica domain sizes.

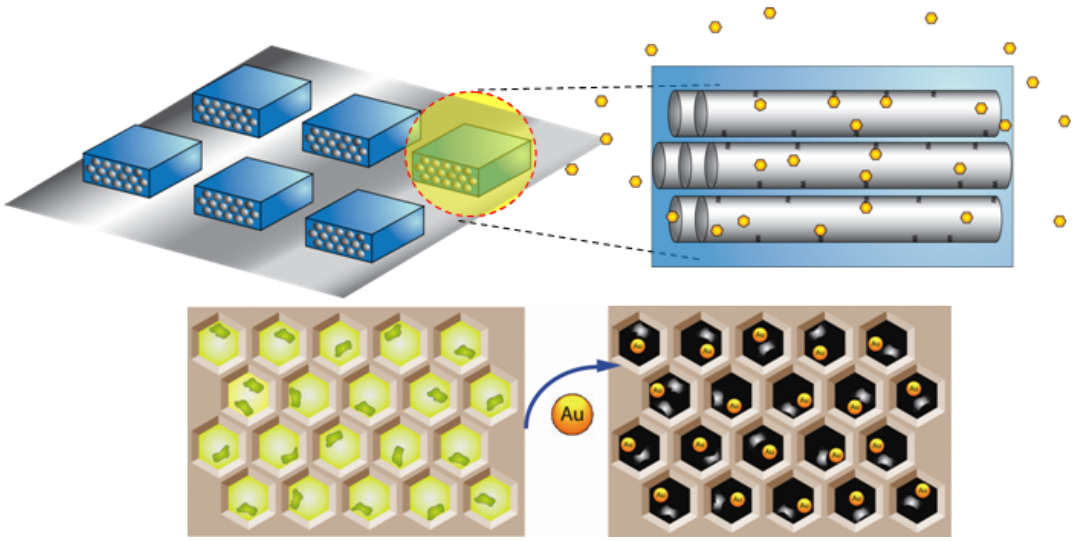

Figure 5.3: Schematic representation of gold nanoparticles penetrating nanochannels to quench the fluorescent dye.

The accessibility of mesochannels in the silica pattern offers an opportunity to regulate diffusion of particles based on relative sizes of these particles compared to the mesopores. We performed several fluorescence-quenching experiments of dye-infused silica films by gold nanoparticles (GNPs) with various sizes to verify the size-

exclusion effect. Gold nanoparticles are well known for their superb ability as fluorescence quenchers. GNPs that are smaller than the pore diameter can freely diffuse into the channels and quench the fluorescence of entire mesoporous films. Larger sized GNPs are excluded from channels and can only quench fluorophores adsorbed on the external surface. Two populations of water-soluble GNPs with 2 nm (monolayer protected) and 14 nm (citrate stabilized) cores were synthesized according to reported methods.[8, 9] Since the quenching ability of GNPs to fluorophores is dependent on particle sizes, we studied quenching efficiency of each GNP against Rhodamine 6G dye in solution to ensure that two separate samples are comparable using a fluorescence spectrophotometer. As indicated in Figure 5.2, the fluorescence intensity of the Rhodamine 6G solution significantly decreased in the presence of GNP-14 nm at 2.37 nM. However, GNP-2 nm at the same concentration only quenched 2% of fluorescence. The GNP-2 nm solution with higher concentration (16 μM) successfully quenched the fluorescence. The quenching efficiency of GNP-14 nm exceeds 6.7×10^3 times than that of GNP-2 nm for the Rhodamine 6G dye in the examined concentration range.

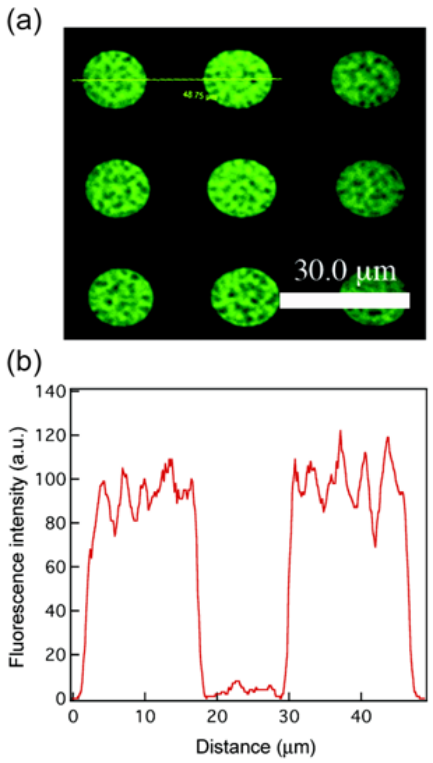

Figure 5.4: (a) The fluorescence image of mesoporous silica patterns after uptaking Rhodamine 6G dye was obtained by confocal LSM. (b) The line profile displays the dye distribution inside the feature.

Quenching experiments of Rhodamine 6G infused mesoporous silica films were based on the optimized concentrations of each of the GNP quenchers. The dye-infused mesoporous patterns prepared from F127 were placed in GNP-2 nm solution displayed considerable quenching of fluorescence after soaking in the GNP solution for 2 days. However, the fluorescence intensity of the same film in GNP-14 nm solution only slightly decreased due to the surface quenching by GNPs (Figure 5.5). Considering bulkiness of large GNPs, the absence of quenching phenomena in GNP-14 nm solution might also originate from hindered diffusion. Therefore, the mesoporous silica film was further immersed in the GNP-14 nm solution for 2 weeks. The resulting film continues to exhibit moderate fluorescence intensity, which

eliminates this possibility (Figure 5.6a). A patterned silica film synthesized from Pluronic F108 template consists of isolated spherical voids in the silica matrix. These closed voids are not accessible to the GNPs. This silica film can be thought of as a "pseudo solid" material. The solution of GNP-14 nm should be able to quench fluorescence of surface adsorbed dyes on this control sample. Before the introduction of GNPs, F108-templated silica patterns in Rhodamine 6G dye displayed strong fluorescence. However, as predicted the fluorescence was significantly quenched after immersion of the F108 sample in the GNP-14 nm solution (Figure 5.6b). Combined with the aforementioned observations, we demonstrated control of substrate diffusion in and out of porous structures physically constrained by pore entrance.

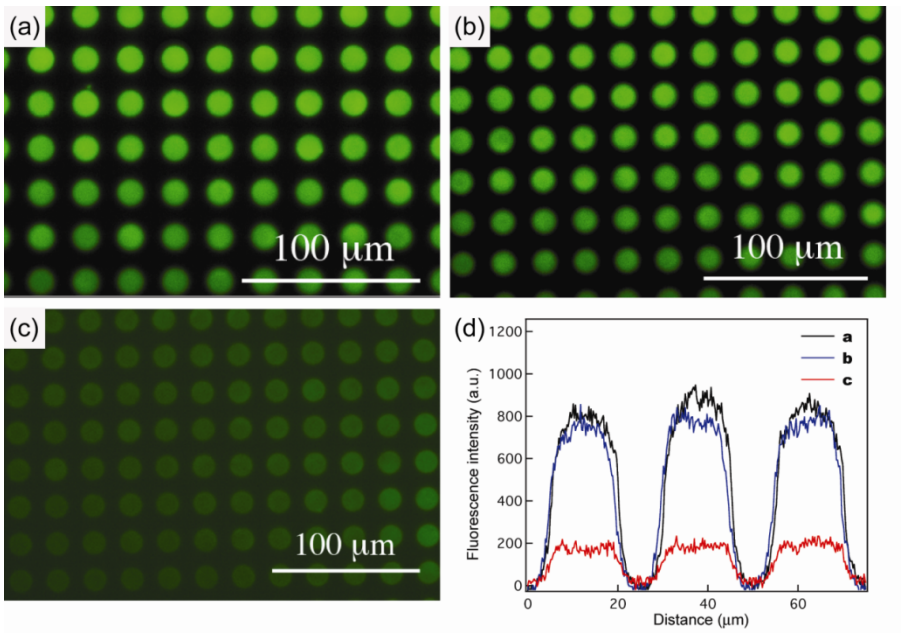

Figure 5.5: (a) The fluorescence image of dye-infused (Rhodamine 6G = 0.1 μM) mesoporous silica patterns synthesized from F127. Fluorescence images of mesoporous silica patterns after soaking with (b) GNP-14 nm (2.37 nM) and (c) GNP-2 nm (16 μM), respectively. (d) Line profile comparing the intensity of mesoporous silica patterns (a), (b) and (c).

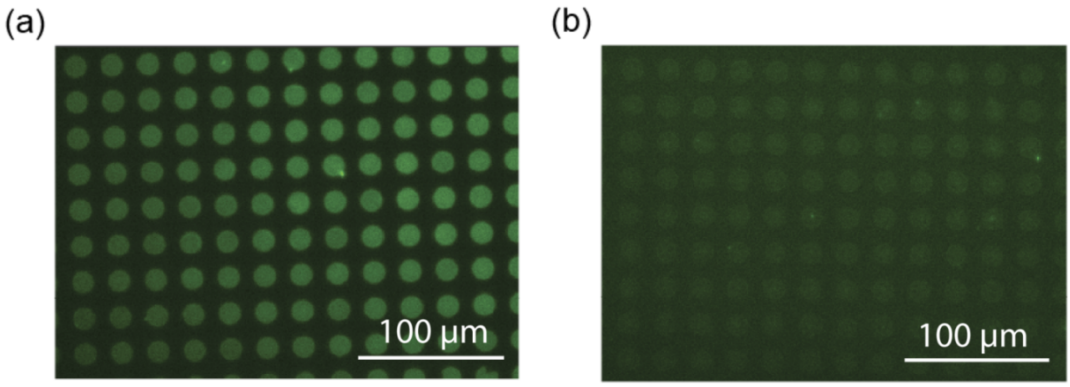

Figure 5.6: (a) A mesoporous silica pattern prepared from F127 that was soaked for 2 weeks in GNP-14 nm (2.37 nM). (b) Sample prepared from F108 after soaking with GNP-14 nm (16 µM) for 2 weeks.

5.4 Conclusions

In this chapter it was shown that the patterned mesoporous structures developed within this dissertation can be utilized as devices. Well-ordered mesoporous silica structures with cylindrical pores of approximately 7-8 nm in diameter were shown to prevent diffusion of nanoparticles larger than the domain size (GNP-14 nm), but allow those that are smaller (GNP-2 nm). It is possible to dial-in a range of sizes by changing the amphiphilic copolymer template. Furthermore, these processes described here can generate arbitrary device-scale geometries that are separate from that of mesoporous (template) morphology. Modification or doping of these surfaces will also enhance sensing and separation utility. These devices are prerequisites to more complicated sensors and nanofluidic separation materials.

5.5 References

(1) B. J. Melde, B. J. Johnson, P. T. Charles, *Sensors* 2008, 8, 5202-5228.

(2) R. Karnik, K. Castelino, C. Duan, R. Fan, P. Yang, A. Majumdar. *Nanofluidic Devices for Sensing and Flow Control*. in *Proceedings of the 4th International Conference on Nanochannels, Microchannels and Minichannels*. 2006. Limerick, Ireland.

(3) A. Yamaguchi, N. Teramae, *Analytical Sciences* 2008, 24, 25-30.

(4) E. T. Knobbe, B. Dunn, P. D. Fuqua, F. Nishida, *Applied Optics* 1990, 29, 2729-2733.

(5) L. Malfatti, T. Kidchob, D. Aiello, R. Aiello, F. Testa, P. Innocenzi, *The Journal of Physical Chemistry C* 2008, 112, 16225-16230.

(6) D. Avnir, D. Levy, R. Reisfeld, *The Journal of Physical Chemistry* 1984, 88, 5956-5959.

(7) G. Zhu, V. I. Gavrilenko, M. A. Noginov, *The Journal of Chemical Physics* 2007, 127, 104503.

(8) K. C. Grabar, R. G. Freeman, M. B. Hommer, M. J. Natan, *Analytical Chemistry* 1995, 67, 735-743.

(9) A. Verma, J. M. Simard, J. W. E. Worrall, V. M. Rotello, *Journal of the American Chemical Society* 2004, 126, 13987-13991.

CHAPTER 6

CONCLUSIONS AND FUTURE WORK

6.1 Conclusions

This dissertation has described a unique method for developing multi-scale devices where it is possible to dial-in the nanoscale morphology while retaining the ability to pattern arbitrary geometries. Well-ordered cylindrical channels of sizes ranging from 3 to 8 nm where generated with pattern size scales ranging from 20 μm to 400 nm. Device feasibility was demonstrated by preventing or allowing diffusion of gold nanoparticles of differing sizes. The projects completed within are precursor experiments that will lead to development of more complex devices. Additional topics and possible routes of study that will expand upon that which was already are described below.

6.1.1 Device Fabrication Technique

When designing a device utilizing this process, the first step is to choose an amphiphilic copolymer template. Options to consider are pore size (governed by molecular weight), type of morphology (governed by volume ratio and Flory-Huggins parameter). Hydrogen bonding additives can be used to order the polymer and slightly adjust the pore size. The next step is to print and replicate the pattern via supercritical carbon dioxide mediated metal oxide infusion. The advantage here is that the template,

patterning and the infusions are separate events enabling a wider range of choices. The ordered template will not be disturbed and films up to a few microns thick can be infused. It is also important to note that this process is not limited to silica and any metal oxide can be infused.

6.1.2 Device Feasibility

Feasibility was examined using a simple multi-sclaed device that tracked fluorescence quenching of rhodamine 6G dye using gold nanoparticles of differing diameters. Diffusion of particles larger (14-16 nm) than the channel diameter (7-8 nm) was prevented while smaller particles (3-5 nm) were able to penetrate the pores and quench the dye. This shows that the devices are functioning and enables further pursuit. It would be simple to expand what was developed here and be able to separate particles/larger biomolecules of various sizes. Note that rigidity and shape should also be considered when attempting to separate moieties of different sizes. In addition, it is important to realize the stresses and forces on the particle being separated to avoid sample destruction.

The device geometry is purely dependent on the lithographic mask or mold. The master mold/mask can be as complex as one developed with e-beam or as simple as a plastic DVD insert as used in this thesis. Mask availability will be situational and the processes described here are independent of mask type. The next step is to place this incorporate a device into an already functioning system or develop an independent sensor or micro/nanofluidic device

6.2 Future Work

6.2.1 Alternate PEO-PPO Systems

It was mentioned previously that any amphiphilic diblock copolymer is a potential candidate for the processes described within this dissertation. However, as also shown here, PEO-b-PPO-b-PEO surfactants form well-ordered cylindrical morphologies with the addition of PAA. There are only three molecular weight sizes available from BASF and ordering other amphihilic templates to the degree of PEO-PPO has shown to be non-trivial. The next logical step would be to synthesize PEO-PPO diblocks/triblocks that span an even greater range of molecular weights. These should follow the same trends as previously discovered for F127, F 87, and F 77 and greatly expand device fabrication options and utility.

6.2.2 Surface Modification

It is also possible to modify the surface of the features as well as modify the pores. For example, small molecules such as HMDS can be used to make the surfaces hydrophobic. This can be introduced using supercritical CO_2 or through an HMDS priming oven. It is also possible to deposit brushes on the surfaces to add further degrees of functionality. If the substrate itself is modified it may be possible to enhance adhesion or direct morphology. Depositing PHEMA or PAA brushes on the surface is a potential route to pattern (and order) PEO-PPO using nanolimprint lithography.

6.2.3 Doping

Addition of metal dopants or nanoparticles can enhance or completely change which moleculars can be segregated or sensed. Numerous dopants and modifications have already been used with mesoporous silica structures.[1] Furthermore, it was also shown that exposure to metal vapors can deposit nanoparticles which direct morphology and add functionality within a PMMA-PHEMA film.[2] This could be followed with a supercritical fluid mediated infusion to form hybrid materials.

6.3 References

(1) B. J. Melde, B. J. Johnson, P. T. Charles, *Sensors* 2008, 8, 5202-5228.

(2) D. Yin, S. Horiuchi, T. Masuoka, *Chemistry of Materials* 2005, 17, 463-469.

BIBLIOGRAPHY

Abate, A. R., D. Lee, T. Do, C. Holtze, D. A. Weitz, *Lab on a Chip* **2008**, 8, 516-518.

Aissou, K., M. Kogelschatz, T. Baron, P. Gentile, *Surface Science* **2007**, 601, 2611-2614.

Alvarez, S. D., A. M. Derfus, M. P. Schwartz, S. N. Bhatia, M. J. Sailor, *Biomaterials* **2009**, 30, 26-34.

Avnir, D., D. Levy, R. Reisfeld, *The Journal of Physical Chemistry* **1984**, 88, 5956-5959.

Bates, F. S., G. H. Fredrickson, *Physics Today* **1999**, 52, 32-38.

Becker, M. L., J. Liu, K. L. Wooley, *Chemical Communications* **2003**, 802.

Behl, M., J. Seekamp, S. Zankovych, C. M. S. Torres, R. Zentel, J. Ahopelto, *Advanced Materials* **2002**, 14, 588-591.

Benahmed, A., R. Lam, N. Rechner, C.-M. Ho, *Journal of Micro/Nanolithography, MEMS and MOEMS* **2007**, 6, 023007-5.

Bertolo, J. M. B., A. Generosi, A. Palummo, L. Albertini, V. Rossi, *Sensors and Actuators B* **2005**, 111-112, 145-149.

Birkefeld, L. D., A. M. Azad, S. A. Akbar, *Journal of the American Ceramic Society* **1992**, 75, 2964-2968.

Blackburn, J. M., D. P. Long, A. Cabanas, J. J. Watkins, *Science* **2001**, 294, 141-145.

Blasco, X., D. Hill, M. Porti, M. Nafria, X. Aymerich, *Nanotechnology* **2001**, 12, 110-112.

Bontempo, D., K. L. Heredia, B. A. Fish, H. D. Maynard, *Journal of the American Chemical Society* **2004**, 126, 15372.

Bontempo, D., H. D. Maynard, *Journal of the American Chemical Society* **2005**, 127, 6508.

Brinker, C. J., Y. F. Lu, A. Sellinger, H. Y. Fan, *Advanced Materials* **1999**, 11, 579-585.

Britcher, L. G., D. C. Kehoe, J. G. Matisons, A. G. Swincer, *Macromolecules* **1995**, 28, 3110-3118.

Brunner, H., T. Vallant, U. Mayer, H. Hoffmann, *Langmuir* **1996**, 12, 4614.

Brust, M., M. Walker, D. Bethell, D. J. Schiffrin, R. Whyman, *Journal of the Chemical Society, Chemical Communications* **1994**, 801-802.

Cabanas, A., E. Enciso, M. C. Carbajo, M. J. Torralvo, C. Pando, J. A. R. Renuncio, *Chemistry of Materials* **2005**, 17, 6137-6145.

Cabanas A., J. M. Blackburn, J. J. Watkins, *Microelectronic Engineering* **2002**, 64, 53-61.

Cabanas A., D. P. Long, J. J. Watkins, *Chemistry of Materials* **2004**, 16, 2028-2033.

Cagnol, F., D. Grosso, G. Soler-Illia, E. L. Crepaldi, F. Babonneau, H. Amenitsch, C. Sanchez, *Journal of Materials Chemistry* **2003**, 13, 61-66.

Cao, C., A. Y. Fadeev, T. J., McCarthy, *Langmuir* **2001**, 17, 757-761.

Carvalho, E. J., M. A. R. Alves, E. S. Braga, L. Cescato, *Microelectronics Journal* **2006**, 37, 1265-1270.

Chen, H.-T., T. A. Crosby, M.-H. Park, S. Nagarajan, V. M. Rotello, J. J. Watkins, *Journal of Materials Chemistry* **2009**, 19, 70-74.

Cheng, J. Y., C. A. Ross, H. I. Smith, E. L. Thomas, *Advanced Materials* **2006**, 18, 2505-2521.

Choi, P., P.-F. Fu, L. J. Guo, *Advanced Functional Materials* **2007**, 17, 65-70.

Chu, J. P., H. Wijaya, C. W. Wu, T. R. Tsai, C. S. Wei, T. G. Nieh, J. Wadsworth, *Applied Physics Letters* **2007**, 90, 034101-3.

Ciampolini, M., N. Nardi, *Inorganic Chemistry* **1966**, 5, 41-44.

Clark, T., J. D. Ruiz, H. Y. Fan, C. J. Brinker, B. I. Swanson, A. N. Parikh, *Chemistry of Materials* **2000**, 12, 3879-3884.

Combes, J. R., White, L. D., Tripp, C. P., *Langmuir* **1999**, 15, 7870-7875.

Comes, M., M. D. Marcos, R. Martinez-Manez, F. Sancenon, L. A. Villaecusa, A. Graefe,G. J. Mohr, *Journal of Materials Chemistry* **2008**, 18, 5815-5823.

Corma, A., *Chemical Reviews* **1997**, 97, 2373-2419.

Cosnier S, C. Gondran, A. Senillou, M. Gratzel, N. Vlachopoulos, *Electroanalysis* **1997**, 9, 1387-1392.

Dattelbaum, A. M., M. L. Amweg, L. E. Ecke, C. K. Yee, A. P. Shreve, A. N. Parikh, *Nano Letters* **2003**, 3, 719-722.

Davis, M. E., *Nature* **2002**, 417, 813-821.

de Theije, F. K., A. R. Balkenende, M. A. Verheijen, M. R. Baklanov, K. P. Mogilnikov,Y. Furukawa, *Journal of Physical Chemistry B* **2003**, 107, 4280-4289.

Della, G. G., M. Guglielmi, G. Brusatin, M. Prasciolu, F. Romanato, *Journal of Sol-Gel Science and Technology* **2008**, 48, 212-216.

Deng, T., Y.-H. Ha, J. Y. Cheng, C. A. Ross, E. L. Thomas, *Langmuir* **2002**, 18, 6719-6722.

Doshi, D. A., N. K. Huesing, M. C. Lu, H. Y. Fan, Y. F. Lu, K. Simmons-Potter, B. G. Potter, A. J. Hurd, C. J. Brinker, *Science (Washington, D. C., 1883-)* **2000**, 290, 107-111.

Edmondson, S., V. L. Osborne, W. T. S. Huck, *Chemical Society Reviews* **2004**, 33, 14.

Eijkel, J. C. T., A. v. d. Berg, *Microfluidics and Nanofluidics* **2005**, 1, 249-267.

El-Safty, S. A., *Adsorption* **2009**, 15, 227-239.

Errington, R. J., J. Ridland, R., W. Clegg, R. A. Coxall, J. M. Sherwood, *Polyhedron* **1998**, 17, 659-674.

Fadeev, A. Y., T. J. McCarthy, *Journal of the American Chemical Society* **1999**, 121, 12184-12185.

Fan, H. Y., Y. F. Lu, A. Stump, S. T. Reed, T. Baer, R. Schunk, V. Perez-Luna, G. P. Lopez, C. J. Brinker, *Nature* **2000**, 405, 56-60.

Fan, H. Y., S. Reed, T. Baer, R. Schunk, G. P. Lopez, C. J. Brinker, *Microporous and Mesoporous Materials* **2001**, 44, 625-637.

Feng, X., G. E. Fryxell, L.-Q. Wang, A. Y. Kim, J. Liu, K. M. Kemner, *Science* **1997**, 276, 923-926.

Fernandes, N. E., S. M. Fisher, J. C. Poshusta, D. G. Vlachos, M Tsapatsis, J. J. Watkins, *Chemistry of Materials* **2001**, 13, 2023-2031.

Flores-Arias, M. T., A. Castelo, C. Gomez-Reino, G. F. de la Fuente, *Optics Communications* **2009**, 282, 1175-1178.

Ford, J., S. Yang, *Chemistry of Materials* **2007**, 19, 5570-5575.

Gates, B. D., Q. B. Xu, M. Stewart, D. Ryan, C. G. Willson, G. M. Whitesides, *Chemical Reviews* **2005**, 105, 1171-1196.

Ghosh, S. K., A. Pal, S. Kundu, S. Nath, T. Pal, *Chemical Physics Letters* **2004**, 395, 366-372.

Grabar, K. C., R. G. Freeman, M. B. Hommer, M. J. Natan, *Analytical Chemistry* **1995**, 67, 735-743.

Gu, W., C. P. Tripp, *Langmuir* **2006**, 22, 5748-5752.

Guo, L. J., *Advanced Materials* **2007**, 19, 495-513.

Gupta, R. R., V. S. RamachandraRao, J. J. Watkins, *Macromolecules* **2003**, 36, 1295-1303.

Harris, K. D., A. Huizinga, M. J. Brett, *Electrochemical and Solid-State Letters* **2002**, 5, H27-H29.

Hawker, C. J., K. L. Wooley, *Science* **2005**, 309, 1200.

Heredia, K. L., D. Bontempo, T. Ly, J. T. Byers, S. Halstenberg,H. D. Maynard, *Journal of the American Chemical Society* **2005**, 127, 16955.

Hernandez, F. E., S. Yu, M. Garcia, A. D. Campiglia, *The Journal of Physical Chemistry* **2005**, 109, 9499-9504.

Hoffmann, H., U. Mayer, H. Brunner, A. Krischanitz, *Vibrational Spectroscopy* **1995**, 8, 151.

Hoffmann, H., U. Mayer, A. Krischanitz, *Langmuir* **1995**, 11, 1304.

Hong, L.-Y., D.-H. Lee, D.-P. Kim, *Journal of Physics and Chemistry of Solids* **2008**, 69, 1436-1438.

Hong, S. H., J. Zhu, C. A. Mirkin, *Science (Washington, D. C., 1883-)* **1999**, 286, 523-525.

Hozumi, A., H. Sugimura, K. Hiraku, T. Kameyama, O. Takai, *Nano Letters* **2001**, 1, 395-399.

Hu, Z., G. Baralia, V. Bayot, J.-F. Gohy, A. M. Jonas, *Nano Letters* **2005**, 5, 1738-1743.

Hua, C. Y., A. Jagota, Y. Y. Lin, E. J. Kramer, *Langmuir* **2002**, 18, 1394.

Huang, K.-Y., Z.-P. He, K.-J. Chao, *Thin Solid Films* **2006**, 495, 197-204.

Innocenzi, P., T. Kidchob, P. Falcaro, M. Takahashi, *Chemistry of Materials* **2008**, 20, 607-614.

Innocenzi P., P. Falcaro, J. M. Bertolo, A. Bearzotti, H. Amenitsch, *Journal of Non-Crystalline Solids* **2005**, 315, 1980-1986.

Ito, Y., S. Nishi, Y. S. Park, Y. Imanishi, *Macromolecules* **1997**, 30, 5856-5859.

Ito, Y., Y. Ochiai, Y. S. Park, Y. Imanishi, *Journal of the American Chemical Society* **1997**, 119, 1619-1623.

Jain, P., L. Sun, J. Dai, G. L. Baker, M. L. Bruening, *Biomacromolecules* **2007**, 8, 3102-3107.

Jansen, H., H. Gardeniers, M. de Boer, M. Elwenspoek, J. Fluitman, *Journal of Micromechanics and Microengineering* **1996**, 6, 14-28.

Ji, Q., S. B. Yoon, J. P. Hill, A. Vinu, J.-S. Yu, K. Ariga, *Journal of the American Chemical Society* **2009**, 131, 4220-4221.

Jordan, R., A. Ulman, *Journal of the American Chemical Society* **1998**, 120, 243.

Jordan, R., A. Ulman, J. F. Kang, M. H. Rafailovich, J. Sokolov, *Journal of the American Chemical Society* **1999**, 121, 1016.

Jung, D.-H., I. J. Park, Y. K. Choi, S.-B. Lee, H. S. Park, J. Ruhe, *Langmuir* **2002**, 18, 6133-6139.

Kato, M., M. Kamigaito, M. Sawamoto, T. Higashimura, *Macromolecules* **1995**, 28, 1721.

Kato, N., F. Caruso, *The Journal of Physical Chemistry B* **2005**, 109, 19604-19612.

Kawai, T., K. Sugita, K. Saito, T. Sugo, *Macromolecules* **2000**, 33, 1306-1309.

Kawakita, H., H. Masunaga, K. Nomura, K. Uezu, I. Akiba, S. Tsuneda, *Journal of Porous Materials* **2007**, 14, 387-391.

Kim, E., Y. Xia, G. M. Whitesides, *Nature* **1995**, 376, 581-584.

Kim, H. C., C. R. Kreller, K. A. Tran, V. Sisodiya, S. Angelos, G. Wallraff, S. Swanson, R. D. Miller, *Chemistry of Materials* **2004**, 16, 4267.

Knobbe, E. T., B. Dunn, P. D. Fuqua, F. Nishida, *Applied Optics* **1990**, 29, 2729-2733.

Kuhn, S., U. Hakanson, L. Rogobete, V. Sandoghdar, *Physical Review Letters* **2006**, 97, 017402.

Kulkarni, M. M., R. Bandyopadhyaya, A. Sharma, *Journal of Chemical Sciences* **2008**, 120, 637-643.

Lai, Z. P., G. Bonilla, I. Diaz, J. G. Nery, K. Sujaoti, M. A. Amat, E. Kokkoli, O. Terasaki, R. W. Thompson, M. Tsapatsis, D. G. Vlachos, *Science* **2003**, 300, 456-460.

Lecolley, F., L. Tao, G. Mantovani, I. Durkin, S. Lautru, D. M. Haddleton, *Chemical Communications* **2004**, 2026.

Lei C.H., Y. S. Shin, J. Liu, E. J. Ackerman, *Journal of the American Chemical Society* **2002**, 124, 11242-11243.

Lewis, L. N., R. E. Colborn, H. Grade, G. L. Bryant, C. A. Sumpter, R. A. Scott, *Organometallics* **1995**, 14, 2202.

Li, H.-W., W. T. S. Huck, *Nano Letters* **2004**, 4, 1633-1636.

Li M.Q., K. Douki, K. Goto, X. F. Li, C. Coenjarts, D. M. Smilgies, C. K. Ober, *Chemistry of Materials* **2004**, 16, 3800-3808.

Liu, C.-Y., C.-F. Chen, J.-P. Leu, *Journal of the Electrochemical Society* **2009**, 156, J16-J19.

Lu, Y. F., R. Ganguli, C. A. Drewien, M. T. Anderson, C. J. Brinker, W. L. Gong, Y. X. Guo, H. Soyez, B. Dunn, M. H. Huang, J. I. Zink, *Nature* **1997**, 389, 364-368.

Lu, Y. F., Y. Yang, A. Sellinger, M. C. Lu, J. M. Huang, H. Y. Fan, R. Haddad, G. Lopez, A. R. Burns, D. Y. Sasaki, J. Shelnutt, C. J. Brinker, *Nature* **2001**, 410, 913-917.

Lue, S. J., J.-J. Hsu, T.-C. Wei, *Journal of Membrane Science* **2008**, 321, 146-154.

Mair, D. A., T. R. Schwei, T. S. Dinto, F. Svec, J. M. J. Frechet, *Lab on a Chip* **2009**, 9, 877-883.

Malfatti, L., S. Costacurta, T. Kidchob, P. Innocenzi, M. Casula, H. Amenitsch, D. Dattilo, M. Maggini, *Microporous and Mesoporous Materials* **2009**, 120, 375-380.

Malfatti, L., T. Kidchob, D. Aiello, R. Aiello, F. Testa, P. Innocenzi, *The Journal of Physical Chemistry C* **2008**, 112, 16225-16230.

Malfatti, L., T. Kidchob, S. Costacurta, P. Falcaro, P. Schiavuta, H. Amenitsch, P. Innocenzi, *Chemistry of Materials* **2006**, 18, 4553-4560.

Mateeva, E. G., T. Shtoyko, I. Gryczynski, I. Akopova, Z. Gryczynski, *Chemical Physical Letters* **2008**, 454, 85-90.

McCool, B., C. P. Tripp, *Journal of Physical Chemistry B* **2005**, 109, 8914-8919.

Melde, B. J., B. J. Johnson, P. T. Charles, *Sensors* **2008**, 8, 5202-5228.

Mirkin, C. A., *Science* **1999**, 286, 2095-2096.

Moran, I. W., A. L. Briseno, S. Loser, K. R. Carter, *Chemistry of Materials* **2008**, 20, 4595-4601.

Moran, I. W., D. F. Cheng, S. B. Jhaveri, K. R. Carter, *Soft Matter* **2008**, 4, 168-176.

Mougenot, M., M. Lejeune, J. F. Baumard, C. Boissiere, F. Ribot, D. Grosso, C. Sanchez, R. Noguera, *Journal of the American Ceramic Society* **2006**, 89, 1876-1882.

Mukherjee, R., A. Sharma, G. Patil, D. Faruqui, P. Sarathi, G. Pattader, *Bulletin of Materials Science* **2008**, 31, 249-261.

Nagarajan, S., J. K. Bosworth, C. K. Ober, T. P. Russell, J. J. Watkins, *Chemistry of Materials* **2008**, 20, 604-606.

Nagarajan, S., L. M., R. A. Pai, J. K. Bosworth, P. Busch, D. M. Smilgies, C. K. Ober, T. P. Russell,J. J. Watkins, *Advanced Materials* **2008**, 20, 246-251.

Nagarajan, S., T. P. Russell, J. J. Watkins, *Advanced Functional Materials* **2009**, 19, 1-7.

Nau, W. M., J. Mohanty, *International Journal of Photoenergy* **2005**, 7, 133-141.

Nie, Z., E. Kumacheva, *Nature Materials* **2008**, 7, 277-290.

Niranjan R. S., V. A. Chaudhary, I. S. Mulla, K. Vijayamohanan, Sensors and Actuators B-Chemical **2002**, 85, 26-32.

O'Neil, A. S., R. Mokaya, M. Poliakoff, *Journal of the American Chemical Society* **2002**, 124, 10636 - 10637.

Pai, R. A., R. Humayun, M. T. Schulberg, A. Sengupta, J.-N. Sun, J. J. Watkins, *Science* **2004**, 303, 507-510.

Pai, R. A., J. J. Watkins, *Advanced Materials* **2006**, 18, 241-245.

Paik, J. A., S. K. Fan, C. J. Kim, M. C. Wu, B. Dunn, *Journal of Materials Research* **2002**, 17, 2121-2129.

Paul, A., M. Sarkar, D. C. Khara, T. Kamijo, A. Yamaguchi, N. Teramae, A. Samanta, *Chemical Physics Letters* **2009**, 469, 71-75.

Paulose, M., O. K. Varghese, G. K. Mor, C. A. Grimes, K. G. Ong, *Nanotechnology* **2006**, 17, 398-402.

Percec, V., B. Barboiu, H. J. Kim, *Journal of the American Chemical Society* **1998**, 120, 305.

Pierre, A. C., E. Elaloui, G. M. Pajonk, *Langmuir* **1998**, 14, 66-73.

Piner, R. D., J. Zhu, F. Xu, S. H. Hong, C. A. Mirkin, *Science* **1999**, 283, 661-663.

Ray, P. C., A. Fortner, J. Griffin, C. K. Kim, J. P. Singh, H. Yu, *Chemical Physics Letters* **2005**, 414, 259-264.

Rusconi, R., H. A. Stone, *Physical Review Letters* **2008**, 101, 254502-1 - 254502-4.

Sanchez, C., C. Boissiere, D. Grosso, C. Laberty, L. Nicole, *Chemistry of Materials* **2008**, 20, 682-737.

Sayari, A., S. Hamoudi, *Chemistry of Materials* **2001**, 13, 3151-3168.

Schepelina, O., I. Zharov, *Langmuir* **2007**, 23, 12704-12709.

Schift, H., *Journal of Vacuum Science & Technology B: Microelectronics and Nanometer Structures* **2008**, 26, 458-480.

Schneider, G., G. Decher, *Nano Letters* **2006**, 6, 530-536.

Schuth, F., W. Schmidt, *Advanced Materials* **2002**, 14, 629-638.

Scott, B. J., G. Wirnsberger, G. D. Stucky, *Chemistry of Materials* **2001**, 13, 3140-3150.

Shih, T.-K., J.-R. Ho, H.-Y. Liao, C.-F. Chen, C.-Y. Liu, *Thin Solid Films* **2008**, 516, 5339-5343.

Slavov, S. V., A. R. Sanger, K. T. Chuang, *Journal of Physical Chemistry B* **2000**, 104, 983-989.

Stallings, W. E., and H. H. Lamb, *Langmuir* **2003**, 19, 2989-2994.

Stein, A., *Advanced Materials* **2003**, 15, 763-775.

Striemer, C. C., T. R. Gaborski, J. L. McGrath, P. M. Fauchet, *Nature* **2007**, 445, 749-753.

Sugimura, H., A. Hozumi, T. Kameyama, O. Takai, *Advanced Materials* **2001**, 13, 667-670.

Sun, L., J. Dai, G. L. Baker, M. L. Bruening, *Chemistry of Materials* **2006**, 18, 4033-4039.

Tan, L., Z. Ouyang, M. Liu, J. Ell, J. Hu, T. E. Patten, G.-Y. Liu, *The Journal of Physical Chemistry B* **2006**, 110, 23315-23320.

Tetelin, A., Pellet, C., Laville, C., and N'Kaoua, G., *Sensors and Actuators B* **2003**, 91, 211-218.

Tetelin, A., V. Pouget, J.-L. Lachaud, C. Pellet, *IEEE Transactions on Instrumentation and Measurement* **2004**, 53, 1262-1267.

Tirumala, V. R., R. A. Pai, S. Agarwal, J. J. Testa, G. Bhatnagar, A. H. Romang, C. Chandler, B. P. Gorman, R. L. Jones, E. K. Lin, J. J. Watkins, *Chemistry of Materials* **2007**, 19, 5868-5874.

Trau, M., N. Yao, E. Kim, Y. Xia, G. M. Whitesides, I. A. Aksay, *Nature* **1997**, 390, 674-676.

Tripp, C. P., J. R. Combes, *Langmuir* **1998**, 14, 7348-7352.

Tu, J., R. Wang, W. Geng, X. Lai, T. Zhang, N. Li, N. Yue, X. Li, *Sensors and Actuators B* **2009**, 136, 392-398.

Vallant, T., H. Brunner, U. Mayer, H. Hoffmann, T. Leitner, R. Resch, *J. Phys. Chem. B.* **1998**, 102, 7190.

Varghese, O. K., and C. A. Grimes, *Journal of Nanoscience and Nanotechnology* **2003**, 3, 277-293.

Varghese, O. K., D. Gong, M. Paulose, K. G. Ong, and C. A. Grimes, *Sensors and Actuators B* **2003**, 93, 338-344.

Varghese O.K., X. P. Yang, J. Kendig, M. Paulose, K. F. Zeng,C. Palmer, K. G. Ong, C. A. Grimes, *Sensor Letters* **2006**, 4, 120-128.

Verma, A., J. M. Simard, J. W. E. Worrall, V. M. Rotello, *Journal of the American Chemical Society* **2004**, 126, 13987-13991.

Vieu, C., F. Carcenac, A. Pépin, Y. Chen, M. Mejias, A. Lebib, L. Manin-Ferlazzo, L. Couraud, H. Launois, *Applied Surface Science* **2000**, 164, 111-117.

Vogt, B. D., R. A. Pai, H.-J. Lee, R. C. Hedden, C. L. Soles, W.L. Wu, E. K. Lin, B. J. Bauer, J. J. Watkins, *Chemistry of Materials* **2005**, 17, 1398-1408.

von Werne, T., T. E. Patten, *Journal of the American Chemical Society* **2001**, 123, 7497.

Waitz, T., T. Wagner, T. Sauerwald, C.-D. Kohl, M. Tiemann, *Advanced Functional Materials* **2009**, 19, 653-661.

Wakayama, H., H. Itahara, N. Tatsuda, S. Inagaki, Y. Fukushima, *Chemistry of Materials* **2001**, 13, 2392 - 2396.

Walcarius, A., *Electroanalysis* **1998**, 10, 1217-1235.

Wang, C.-T., C. L. Wu, *Thin Solid Films* **2006**, 496, 658-664.

Wang, C. T., C. L. Wu, I. C. Chen,Y. H. Huang, *Sensor and Actuators B - Chemical* **2005**, 107, 402-410.

Wang, F., J. Yang, K. Wu, *Analytica Chimica Acta* **2009**, 638, 23-28.

Wang, L., D. Li, R. Wang, Y. He, Q. Qi, Y. Wang, T. Zhang, *Sensors and Actuators B* **2008**, 133, 622-627.

Watkins, J.J., J. M. Blackburn, T. J. McCarthy, *Chemistry of Materials* **1999**, 11, 213-215.

White, C. E., C. L. Henderson, *Proceedings of SPIE* **2004**, 5376, 850 - 860.

Wickramanayaka, S., Y. Nakanishi, Y. Hatanaka, *Applied Surface Science* **1997**, 113-114, 670-674.

Wirnsberger, G., B. J. Scott, G. D. Stucky, *Chemical Communications* **2001**, 119-120.

Wirnsberger, G., P. D. Yang, B. J. Scott, B. F. Chmelka, G. D. Stucky, *Spectrochimica Acta, Part A: Molecular Spectroscopy* **2001**, 57, 2049-2060.

Wu, C. W., T. Aoki, M. Kuwabara, *Nanotechnology* **2004**, 15, 1886-1889.

Wu, J.-C., Y. Wang, C.-C. Chen, Y.-C. Chang, *Chemistry of Materials* **2008**, 20, 6148-6156.

Xia, Y., M. Mrksich, E. Kim, G. M. Whitesides, *Journal of the American Chemical Society* **1995**, 117, 9576-9577.

Xia, Y. N., G. M. Whitesides, *Annual Review of Materials Science* **1998**, 28, 153-184.

Yamaguchi, A., N. Teramae, *Analytical Sciences* **2008**, 24, 25-30.

Yang, D., S. W. Chang, C. K. Ober, *Journal of Materials Chemistry* **2006**, 16, 1693-1696.

Yang, P. D., T. Deng, D. Y. Zhao, P. Y. Feng, D. Pine, B. F. Chmelka, G. M. Whitesides,G. D. Stucky, *Science* **1998**, 282, 2244-2246.

Yang, P. D., A. H. Rizvi, B. Messer, B. F. Chmelka, G. M. Whitesides, G. D. Stucky, *Advanced Materials* **2001**, 13, 427-431.

Yang, P. D., G. Wirnsberger, H. C. Huang, S. R. Cordero, M. D. McGehee, B. Scott, T. Deng, G. M. Whitesides, B. F. Chmelka, S. K. Buratto, G. D. Stucky, *Science* **2000**, 287, 465-467.

Yang, X., Y. Xu, K. Lee, S. Xiao, D. Kuo, D. Weller, *IEEE Transactions on Magnetics* **2009**, 45, 833-838.

Yin, D., S. Horiuchi, T. Masuoka, *Chemistry of Materials* **2005**, 17, 463-469.

Yuliarto, B., Y. Kumai, S. Inagaki, H. Zhou, *Sensors and Actuators B* **2009**, 138, 417-421.

Zeng, Y.,D. J. Harrison, *Analytical Chemistry* **2007**, 79, 2289-2295.

Zhang, J., S. Wang, Y. Wang, Y. Wang, B. Zhu, H. Xia, X. Guo, S. Zhang, W. Huang, S. Wu, *Sensors and Actuators B* **2009**, 135, 610-617.

Zhao, B., W. J. Brittain, *Journal of the American Chemical Society* **1999**, 121, 3557.

Zhao, B., L. Zhu, *Journal of the American Chemical Society* **2006**, 128, 4574.

Zhu, G., V. I. Gavrilenko, M. A. Noginov, *The Journal of Chemical Physics* **2007**, 127, 104503.